Title: Entry by multiple picornaviruses is dependent on a pathway that includes TNK2, WASL and NCK1

Hongbing Jiang[1]#, Christian Leung[1], Stephen Tahan[1], David Wang[1]#

1 Department of Molecular Microbiology, Pathology and Immunology, Washington University in St. Louis, School of medicine, St. Louis, MO, 63110

#Address correspondence to:

Hongbing Jiang and David Wang

Washington University in St. Louis School of Medicine

Campus box 8230

660 S. Euclid Ave.

St. Louis, MO 63110 USA

Email: davewang@wustl.edu, hongbingjiang@wustl.edu

Word count: abstract 148;

Page number 50, line number 812

Abstract

Comprehensive knowledge of the host factors required for picornavirus infection would facilitate antiviral development. Here we demonstrate roles for three human genes, TNK2, WASL, and NCK1, in infection by multiple picornaviruses. CRISPR deletion of TNK2, WASL or NCK1 reduced encephalomyocarditis virus (EMCV), coxsackievirus B3 (CVB3), poliovirus and enterovirus D68 infection, and chemical inhibitors of TNK2 and WASL decreased EMCV infection. Reduced EMCV lethality was observed in mice lacking TNK2. TNK2, WASL and NCK1 were important in early stages of the viral lifecycle, and genetic epistasis analysis demonstrated that the three genes function in a common pathway. Mechanistically, reduced internalization of EMCV was observed in TNK2 deficient cells demonstrating that TNK2 functions in EMCV entry. Domain analysis of WASL demonstrated that its actin nucleation activity was necessary to facilitate viral infection. Together, these data support a model wherein TNK2, WASL, and NCK1 comprise a pathway critical for multiple picornaviruses.

Introduction

Picornaviruses cause a wide range of diseases including the common cold, hepatitis, myocarditis, poliomyelitis, meningitis, and encephalitis (1). Although vaccines exist for poliovirus and hepatitis A virus, there are currently no FDA approved antivirals against picornaviruses in the United States. As obligate intracellular pathogens, viruses are dependent on the host cellular machinery to complete their lifecycle. Targeting of such host cellular factors in the design of antiviral drugs can circumvent resistance that arises from rapid mutation of viruses. The early stages of the virus lifecycle, including receptor binding,

41 entry, uncoating, and initiation of replication, are the ideal targets for preventing virus infection since
42 the virus has not yet multiplied.

43 Despite extensive studies (2), there remain significant gaps in our understanding of virus entry.
44 As the family *Picornaviridae* encompasses a wide range of viruses, it is not surprising that there is
45 diversity in the known entry mechanisms of different species. Among the picornaviruses, poliovirus
46 entry has been the most extensively studied. While some reports suggest that poliovirus enters the cell
47 through clathrin-mediated endocytosis and that its genome release depends on endosome acidification
48 (3), more recent studies report that poliovirus enters cells by a clathrin-, caveolin-, flotillin-, and
49 microtubule-independent pathway (4). Furthermore, poliovirus entry is sensitive to inhibitors of both
50 tyrosine kinases and actin-polymerization, although it is not known which specific tyrosine kinase(s)
51 is/are critical for poliovirus infection (4). Coxsackie virus B3 (CVB3) entry has also been extensively
52 studied (5). In polarized epithelial cells, CVB3 binding to the co-receptor decay-accelerating factor (DAF)
53 and the coxsackievirus and adenovirus receptor (CAR) leads to entry by caveolin-dependent endocytosis
54 and macropinocytosis (6, 7). In contrast to CVB3 and poliovirus, there have been few studies of EMCV
55 entry. Vascular cell adhesion molecule 1 (VCAM-1) is reported to be a receptor for EMCV (8). Interaction
56 of the EMCV virion with VCAM-1 is believed to induce a conformational change that then releases the
57 viral RNA genome; entry into the cytosol is reported to be independent of acidification (9).

58 Using a novel virus infection system comprised of the model organism *C. elegans* and Orsay
59 virus, the only known natural virus of *C. elegans*, we previously identified several genes that are
60 essential for virus infection in *C. elegans* (10). The genes *sid-3*, *viro-2* and *nck-1* were found to be
61 essential for an early, pre-replication step of the Orsay virus lifecycle. *sid-3* encodes a non-receptor
62 tyrosine kinase orthologous to human Tyrosine Kinase Non-Receptor 2 (TNK2), *viro-2* encodes an
63 orthologue of human Wiskott-Aldrich Syndrome protein Like protein (WASL), and *nck-1* encodes an

64 orthologue of Non-Catalytic Region of Tyrosine Kinase (NCK1), an adaptor protein that binds to both
65 TNK2 and WASL (11, 12). Since Orsay virus is a non-enveloped, positive strand RNA virus that is
66 evolutionarily related to the family *Picornaviridae*, we reasoned that the human orthologues of these
67 genes may have a conserved role in infection by picornaviruses.

68 Human TNK2 is linked to cancers, has been reported to be activated by multiple extracellular
69 stimuli, and is involved in many different pathways, such as clathrin/receptor mediated endocytosis,
70 regulation of EGFR degradation, transduction of signals into the nucleus, and regulation of actin
71 polymerization (11, 13-15). Furthermore, overexpression of TNK2 induces interferon and leads to
72 reduced replication of a Hepatitis C virus replicon (16). To date, there are no publications demonstrating
73 a positive role for TNK2 in virus infection; several siRNA based screens suggest that TNK2 is important
74 for influenza A virus (IAV), vesicular stomatitis virus (VSV), and hepatitis C virus (HCV) infections (16-19),
75 but no validation of these screening results have been reported. Humans encode two orthologues of
76 *viro-2*, WASP and WASL (Wiskott-Aldrich syndrome protein/-like) (20). Strikingly, biochemical assays
77 have demonstrated that WASL is a substrate for the kinase activity of TNK2 (15), suggesting that the two
78 function in a pathway. NCK1 is an adaptor protein reported to co-localize with TNK2 (11, 21) and
79 interact with WASL. There are only limited studies linking WASL and NCK1 to virus infection. A clear role
80 has been established for WASL in spread of vaccinia virus (22) that involves NCK1 as well (12, 23).
81 Furthermore, sensitivity of Lassa virus infection to Wiskostatin, a small molecule inhibitor of WASL,
82 suggests a role of WASL in virus entry (24). However, there are no studies implicating NCK1 in any aspect
83 of picornavirus infection or in entry of any virus.

84 Here, we determined whether these three human orthologues of the genes found in a *C.*
85 *elegans* forward genetic screen function in an evolutionarily conserved manner to facilitate virus
86 infection in human cell culture. CRISPR-Cas9 genome editing was used to generate knockout cells for

each gene, and their impact on infection by a panel of viruses from different families was then tested. Significant reductions in infection by multiple picornaviruses were observed in each of the cell lines. Consistent with these *in vitro* data, we observed increased survival of mice lacking murine TNK2 after EMCV challenge *in vivo*. We further demonstrated that TNK2, WASL and NCK1 function in a pathway to support EMCV virus infection with WASL and NCK1 lying downstream of TNK2. Mechanistically, loss of TNK2 led to reduced EMCV virus internalization, while both TNK2 and WASL were required for proper endocytic trafficking of EMCV. These data support a model wherein TNK2, WASL and NCK1 comprise a pathway that is critical for entry by multiple picornaviruses.

Results

Non-receptor tyrosine kinase TNK2 is critical for infection by multiple picornaviruses

To investigate the function of TNK2 in virus infection, human lung epithelial carcinoma A549 cells deficient in TNK2 were generated by CRISPR-Cas9 genome editing (Figure 1A). We tested a panel of viruses including multiple viruses from the family *Picornaviridae,* which are evolutionarily related to Orsay virus (25). In a single step growth analysis, deletion of TNK2 by two independent sgRNAs (TNK2 KO1 and TNK2 KO2 cells) reduced EMCV infection by 93% and 86%, respectively, compared to control cells ($P<0.00001$, Figure 1B). When infected by CVB3, 56% and 48% fewer infected TNK2 KO1 and TNK2 KO2 cells were observed ($P<0.0001$, Figure 1C). In a multi-step growth curve, EMCV titers in the supernatant from TNK2 KO1 were 1660-fold lower at 24 hours post infection ($P<0.01$, Figure 1D). In addition, reduced infectivity in TNK2 KO1 was also observed with both recombinant GFP-EMCV and GFP-CVB3, respectively (Figure 1-figure supplement1 A and B). Furthermore, we examined virus replication complex formation by double stranded RNA immunostaining with the commercial J2 antibody and direct electron microscopy (EM) on EMCV infected cells. We observed fewer cells positive for double stranded

RNA and smaller size of the virus replication complex (Figure 1-figure supplement1 C and D). To corroborate these findings, we analyzed EMCV and CVB3 infection in commercial Hap1 cells (a haploid hematopoietic derived lymphoma cell line) deficient in TNK2. Reductions in infected cells by 24% for EMCV and 30% for CVB3 were observed ($P<0.001$, Figure1-figure supplement2 A and B). Statistically significant reductions in poliovirus infection in both Hap1 and A549 TNK2 knockout cells and reduction in enterovirus D68 infection in A549 cells were also observed (Figure 1-figure supplement2 C, E and F). In contrast, no effect of TNK2 deletion was seen for IAV, parainfluenza virus (PIV5) or adenovirus 5 (Figure 1-figure supplement2 D, G, H and I), demonstrating the apparent specificity of TNK2 for picornavirus infection.

We next attempted to rescue the EMCV infection defect in TNK2 knockout cells by ectopic overexpression of TNK2. However, the complexity of the TNK2 locus (three major isoforms and 22 putative transcript variants (26)) presented challenges, and the reported induction of interferon by TNK2 overexpression (16) may have further complicated interpretation of these experiments. Lentivirus expression of each of the three major TNK2 isoforms (which yielded expression levels of TNK2 much higher than the endogenous levels (Figure 1-figure supplement3 D)) in control A549 cells led to statistically significant reductions in EMCV infection (Figure 1- figure supplement3 A, B and C). In addition, fluorescently tagged TNK2 expression through either direct transfection in 293T cells or lentivirus transduction in A549 cells led to aggregates inside the cytosol (Figure 3-figure supplement2 and Figure 5-figure supplement A). Nevertheless, we consistently observed a small, but statistically significant increase in EMCV virus infection in TNK2 KO1 cells transduced with the canonical isoform 1 as compared to the control cells (Figure 1-figure supplement3 A). We also used an alternative approach to rescue virus infection in TNK2 KO1 cells by reverting the 28 bp deletion in clone TNK2 KO1 using CRISPR-Cas9 with oligonucleotide mediated homologous template directed recombination (HDR); 3 synonymous mutations were included in the template to unambiguously identify a successful repair event (Figure 1-

figure supplement3 H). Screening of 500 single-cell clones yielded one clone that had repaired the TNK2 28 bp deletion allele. However, this process also introduced an insertion of 11 nucleotides in the adjacent intron sequence 9 bp from the nearby splice acceptor (Figure 1-figure supplement3 H). We were able to restore low levels of TNK2 expression in the HDR repaired clone (Figure 1-figure supplement3 G). In this clone, EMCV infected cell percentage and virus titer increased, by 8-fold ($P<0.0001$, Figure 1-figure supplement3 E) and 9- fold ($P<0.01$, Figure 1-figure supplement3 F), respectively as compared to TNK2 KO1 cells.

As a completely independent means of assessing the role of TNK2, we treated A549 cells with Aim-100, a small molecule kinase inhibitor with specificity for TNK2 (27). Aim-100 pre-treatment reduced EMCV infection in a dose dependent manner without affecting cell viability (Figure 1E and data not shown).

WASL, a known substrate of TNK2, is critical for picornavirus infection

The human genome encodes two WASP paralogues, WASP and WASL (also known as N-WASP). In this study, we focused on WASL because WASP is not expressed in epithelial cells such as A549. Clonal WASL knockout A549 cells were generated by CRISPR-Cas9 genome editing (Figure 2A). In a single step growth analysis, WASL KO cells showed 62% reduction in EMCV infected cells as compared to control cells ($P<0.0001$, Figure 2B), while in a multi-step growth curve, WASL KO cells yielded 248-fold reduced virus titers at 24 hours post infection ($P<0.01$, Figure 2D). Ectopic expression of WASL in the WASL KO cells rescued EMCV infection to wild type levels (Figure 2-figure supplement A and B). As with TNK2, we observed fewer cells positive for double stranded RNA by immunostaining and smaller size of the virus replication complex by EM (Figure 1-figure supplement1 C and D). Reduced levels of CVB3, poliovirus and enterovirus D68 infection were observed in these cells (Figures 2C, Figure1-figure supplement2 E, F

157 and M). In addition, independent Hap1 cells deficient in WASL had reduced EMCV, CVB3 and poliovirus
158 infection (Figures 1-figure supplement2 A, B and C). To independently assess the role of WASL during
159 virus infection, we used a small molecule inhibitor of WASL, Wiskostatin (28). Wiskostatin reduced
160 EMCV infection in A549 cells in a dose dependent manner with no apparent decrease of cell viability
161 (Figure 2E and data not shown). These data demonstrate that WASL is critical for multiple picornavirus
162 infection in human cell culture.

163

164 **The signaling adaptor protein NCK1 is also critical for picornavirus infection**

165 Deletion of NCK1 in A549 cells (Figure 2F) reduced the number of EMCV and CVB3 infected cells
166 by 55% and 49%, respectively ($P<0.0001$, Figure 2G and 2H) comparable to the reductions observed in
167 WASL KO cells. By a multi-step growth analysis, NCK1 KO showed 10-fold reduction of EMCV virus titer
168 at 24 hours post infection ($P<0.01$ Figure 2I). Ectopic expression of NCK1 in the NCK1 KO cells rescued
169 EMCV infection to wild type levels (Figure 2-figure supplement C and D). As with TNK2 and WASL, these
170 data demonstrate that NCK1 is critical for multiple picornavirus infection in human cell culture.

171

172 **TNK2, WASL, and NCK1 are components of a common pathway**

173 To determine whether TNK2, WASL, and NCK1 act in a common or distinct pathway for virus
174 infection, we performed genetic epistasis analysis by generating double and triple mutant cell lines
175 (Figure 3-figure supplement1 A). EMCV infection levels and viral titer production in the double and triple
176 knockout lines were the same as observed in the TNK2 KO1 lines (Figure 3A and 3B). The lack of an
177 additive effect suggests that WASL and NCK1 are both in the same genetic pathway as TNK2. Combined
178 with the known ability of TNK2 to phosphorylate WASL (15), these data support a model where TNK2

179 acts upstream of WASL and NCK1. The magnitude of the impact of TNK2 KO1 was greater than that of
180 WASL KO or NCK1 KO, suggesting that TNK2 might work through additional pathways in mediating virus
181 infection besides acting through WASL and NCK1.

182 Because TNK2 phosphorylation of WASL increases it actin nucleation activity (29), we reasoned
183 that it might be possible to complement the TNK2 deficiency by overexpression of WASL.
184 Overexpression of wild type WASL in the TNK2 KO1 A549 cells led to increased EMCV virus infection
185 (Figure 3C). Since constitutively active point mutants of WASL have been described (30, 31) , (Figure 3-
186 figure supplement1 B and C), we next tested whether overexpression of three such constructs in the
187 TNK2 KO cells could further increase virus infection.. A higher level of complementation for all three
188 mutants was observed compared to wild type WASL (Figure 3C). For NCK1, based on its reported binding
189 to WASL and TNK2, we hypothesized that its function is to recruit WASL to TNK2, which could then
190 activate WASL via phosphorylation (15, 32). Thus, we also tested whether constitutively active WASL
191 could complement NCK1 KO. Constitutively active WASL fully rescued the NCK1 KO virus infection
192 phenotype (Figure 3D and Figure 3-figure supplement1 D). Together, these data demonstrated that
193 TNK2, WASL, and NCK1 are in a pathway to support picornavirus infection with WASL and NCK1
194 downstream of TNK2.

195 We further evaluated the interactions between TNK2, WASL and NCK1 using biochemical and
196 biophysical assays. Previous studies had reported interaction between NCK1 and WASL through far
197 Western and pull-down assay (12) and co-localization of TNK2 and NCK1 through protein overexpression
198 (11). Fluorescent protein tagged forms of TNK2, WASL, and NCK1 were individually expressed in 293T
199 cells. WASL and NCK1 both distributed homogenously throughout the cytoplasm, while TNK2 formed
200 puncta in the cytoplasm (Figure 3-figure supplement2), which agreed with previous observations (21,
201 33). To examine potential co-localization, we co-expressed either mCerulean tagged TNK2 or mCerulean

tagged WASL with mVenus tagged NCK1 in 293T cells, respectively. Since NCK1 is an adaptor protein, we reasoned that its interactions with binding partners would likely be relatively stable and therefore more readily detectable. Co-expression of mCerulean tagged TNK2 with mVenus tagged NCK1 re-localized NCK1 into the puncta observed by TNK2 expression alone (Figure 3-figure supplement2 and 3A). Co-expression of mCerulean tagged WASL with mVenus tagged NCK1 showed homogenous distribution in the cytoplasm and co-localization of these two proteins (Figure 3-figure supplement2 and 3A). Further analysis by quantitative FRET demonstrated that WASL and NCK1 had higher FRET efficiency in cells, while TNK2 and NCK1 also had significant, but lower, FRET efficiency (Figure 3-figure supplement 3A and 3B). Consistent with the FRET data, in co-transfected 293T cells, immunoprecipitation of FLAG tagged NCK1 pulled down HA tagged WASL more efficiently than it did Myc tagged TNK2 (Figure 3-figure supplement 3C). Altogether, these data demonstrate that TNK2 and WASL bind directly to NCK1.

TNK2, WASL, and NCK1 affect a pre-replication step of the EMCV lifecycle

To begin dissecting the stage of the EMCV virus lifecycle impacted by TNK2, WASL, and NCK1, we transfected EMCV genomic RNA into the cells to bypass the early stages of the viral lifecycle. The TNK2 KO1, WASL KO, and NCK1 KO cells produced the same titers of EMCV virus as the control cells at 10 hours post transfection (Figure 4A) demonstrating that TNK2, WASL, and NCK1 are dispensable for EMCV replication and post-replication stages of the EMCV lifecycle. Thus, we concluded that all three genes act on an early stage of the viral lifecycle. As a second line of evidence, we determined the impact of adding the TNK2 kinase specific inhibitor Aim-100 before or at varying times after EMCV infection. While Aim-100 pre-treatment reduced EMCV infection, administration after virus inoculation had no effect (Figure 4B), consistent with a role for TNK2 at an early stage of virus infection.

TNK2, but not WASL functions in virus internalization

We examined the impact of TNK2 and WASL deletion on virus binding, virus internalization, pore formation, and viral RNA genome translocation. Following incubation at 4°C for one hour, no difference in virus binding was observed among control, TNK2 KO1, and WASL KO cells (Figure 4C), as assessed by qRT-PCR for EMCV genomic RNA. In contrast, after raising the temperature to 37°C for 30 minutes to allow for internalization of the bound virus particles and then trypsinization to remove uninternalized surface virus particles as described before (34, 35), there was a 46% reduction ($P<0.001$) of intracellular EMCV viral RNA in the TNK2 KO1 cells (Figure 4D). However, no difference in RNA levels was observed in WASL KO cells (Figure 4D). As a complementary approach, we evaluated internalization using fluorescently labeled EMCV virions (Figure 4-figure supplement A and B). 25% fewer EMCV positive TNK2 KO1 cells were observed compared to control cells (Figure 4E and Figure 4-figure supplement B), while no statistical difference was observed in the WASL KO cells (Figure 4E and Figure 4-figure supplement B).

We examined the ability of fluorescently labeled transferrin, a known cargo for clathrin mediated endocytosis, to be endocytosed in both TNK2 KO1 and WASL KO cells. Transferrin was internalized in TNK2 KO1 and WASL KO cells to the same level as in the control cells (Figure 4-figure supplement C and D), consistent with a previous report that knock down of TNK2 has no effect on transferrin endocytosis (36). To further check other general virus entry pathways, we also examined whether macropinocytosis was affected in these cells. FITC conjugated Dextran (7 KDa) is reported to be uptaken by macropinocytosis (24). No defect in uptake of Dextran was observed in TNK2 KO1 cells (Figure 4-figure supplement E and F). In contrast, the WASL KO cells had a 75% reduction in Dextran uptake (Figure 4-figure supplement E and F), which is consistent with the known dependency of macropinocytosis on actin polymerization (37). The Dextran macropinocytosis defect in the WASL KO

248 appears to be unrelated to EMCV infection though since no reduction in either binding or internalization
249 of EMCV was observed.

250 A step that is closely linked to internalization for picornaviruses is virus-induced pore formation,
251 which is required for genome release into the cytoplasm. To assess pore formation, cells were treated
252 with the membrane impermeable translation inhibitor, α-sarcin. Virus-induced pore formation will lead
253 to translation inhibition and reduction of ^{35}S methionine and ^{35}S cysteine incorporation whereas in the
254 absence of pore formation, translation will proceed at wild type levels (38). TNK2 KO1 and WASL KO
255 cells showed no defect in virus pore formation during EMCV infection (Figure 4F). Although a clear
256 defect in EMCV internalization exists in the TNK2 KO1 cells (Figure 4D and 4E), no defect in pore
257 formation was observed. Since the internalization defect in TNK2 KO1 cells is not absolute, pore
258 formation may still occur with sufficient frequency to inhibit translation. Alternatively, pore formation
259 may not necessarily require prior internalization; for example binding of parainfluenza virus alone is
260 sufficient to initiate pore formation at the cell membrane (39). For WASL, no defect in binding,
261 internalization or pore formation was observed in the knockout cells, suggesting that the defect is
262 downstream of these steps. Similarly, a recent report suggests that the human gene PLA2G16 acts at a
263 step of the picornavirus lifecycle that is subsequent to pore formation (40).

264 To determine whether TNK2 or WASL plays any role in downstream viral RNA genome
265 translocation after pore formation, we examined virus induced host protein cleavage after its entry. For
266 some picornaviruses, immediately after translocation of its genome, translation of the incoming positive
267 strand RNA leads to proteolytic cleavage of the host protein eIF4G to shut down host translation (41).
268 Since this activity has not been described for EMCV we used CVB3, which is known to have this activity
269 (42). eIF4G cleavage in presence or absence of a virus genome replication inhibitor guanidine
270 hydrochloride showed no difference in the WASL KO cells as compared to the control cells,

271 demonstrating that WASL does not impact this step of the viral lifecycle. In contrast, we observed a
272 decrease of eIF4G cleavage in TNK2 KO1 cells, suggesting that TNK2 might play a role in this process.
273 Alternatively, the reduced eIF4G cleavage level might simply reflect the reduced level of virus
274 internalization in TNK2 KO1 cells (Figure 4G).

275 **Partial co-localization of TNK2 with labeled EMCV particles**

276 TNK2 is present in endocytic vesicles and colocalizes with the early endosome marker EEA1 (21,
277 33, 36, 43). To visualize TNK2 subcellular localization, we expressed N-terminally GFP tagged TNK2 in
278 the TNK2 KO1 cells. Two different patterns were observed in GFP positive cells: high TNK2 expression
279 formed GFP aggregates inside the cytosol of cells in about 80% of the cell population, which has been
280 described previously (21, 44), and low TNK2 expression inside the cytosol of cells in about 20% of the
281 cell population(Figure 5-figure supplement A and B). Consistent with the native TNK2 rescue, N-
282 terminally GFP tagged TNK2 expression in the TNK2 KO1 cells statistically increased virus infection from
283 17.2% to 22.0% of GFP transduced control cell infection ($P<0.01$, Figure 5-figure supplement D). The
284 modest increase was comparable to that observed with ectopic expression of wild type TNK2. Next, we
285 checked TNK2 localization in cells infected with fluorescently labeled EMCV. In TNK2 KO1 cells with high
286 TNK2 expression that formed aggregates, no GFP-TNK2 co-localization with or in proximity to EMCV was
287 observed. However, in cells with low TNK2 expression, labeled EMCV particles were observed in
288 proximity to or surrounded by GFP-TNK2 (Figure 5A and Figure 5-figure supplement A), presumably in
289 early endosomes. Further quantification demonstrated that about 40% of the EMCV particles were in
290 proximity to GFP-TNK2 in those cells (Figure 5-figure supplement C).

291 WASL is recruited to vaccinia virus vesicles to promote its intracellular trafficking (23). To
292 examine whether EMCV infection recruits WASL as observed for poxvirus, we expressed N-terminal GFP
293 tagged WASL in WASL KO cells. The GFP tagged WASL was functional as it rescued EMCV infection

294 (Figure 5-figure supplement E). Following infection with fluorescently labeled EMCV, no clear
295 recruitment of GFP-WASL to fluorescently labeled EMCV was observed (Figure 5A).

296

297 **EMCV infection is CDC42 dependent but clathrin independent**

298 Both TNK2 and WASL are activated by the upstream CDC42 kinase (11, 36, 45-47), which can be
299 inhibited by pirl1 (24). Pirl1 treatment inhibited EMCV replication at a 10 μM concentration without cell
300 toxicity (Figure 5B and data not shown), suggesting that CDC42 mediates EMCV infection.

301 Since a role for TNK2 in clathrin mediated endocytosis (CME) has been reported (21), we next
302 examined whether the classic CME inhibitors such as dynasore (a canonical inhibitor of dynamin) or
303 pitstop-2 (an inhibitor of clathrin) affect EMCV virus infection. Dynasore and pitstop-2 had no effect on
304 EMCV infection while they inhibited VSV, a virus known to rely predominantly on CME for its entry, in a
305 dose dependent fashion (Figure 5-figure supplement F and G). Together, these data indicate that EMCV
306 infection in A549 cells is dependent on CDC42, which activates TNK2 and WASL, but does not require
307 CME for its entry.

308 **EMCV virions accumulate in early endosomes in the absence of TNK2 or WASP**

309 We next examined colocalization of EMCV with the early endosome marker EEA1. A time course
310 analysis demonstrated that in control cells, the peak colocalization of EMCV with EEA1 occurred at 20
311 minutes post internalization (Figure 5-figure supplement H and I), which was followed by a decrease at
312 30 minutes post internalization. This result is consistent with a previous report that poliovirus entry
313 peaks at 20 minutes post infection (4). In contrast, in both the TNK2 KO1 and WASL KO cells, higher
314 levels of EMCV particles were retained in EEA1 containing vesicles at 30 minutes post internalization

(Figure 5C and D, Figure 5-figure supplement I). Thus, both TNK2 KO1 and WASL KO cells are characterized by increased accumulation of EMCV particles in early endosomes.

EMCV infection is dependent on the activation of WASL and its actin modulating function

The primary known effector function of WASL is nucleation of actin polymerization, which is mediated by binding of its C-terminal domain to the Arp2/3 complex and actin monomers (48). Different domains of WASL are critical for interaction with other proteins that can modulate WASL stability, activation, or function. Because ectopic expression of wild type WASL fully rescued EMCV infection in WASL KO cells, we tested the ability of a series of WASL domain deletion mutant constructs to rescue infection in WASL KO cells (Figure 6A). The basic region that binds with PIP2, the proline rich region that binds with SH3 domain containing proteins, the GTPase binding domain that interacts with CDC-42 kinase, and the acidic domain that is involved in actin binding and polymerization were all required for EMCV infection (Figure 6B and 6C). Interestingly, transduction of the N-terminal WH1 domain truncated mutant increased EMCV infection by 3-fold compared to wild type WASL transduction (Figure 6B). The WH1 domain is reported to bind with WASP interacting proteins (WIPs) to maintain WASL in an inactivated state (49); therefore, the WH1 domain truncation mutant should have increased actin polymerization activity. To further assess the WASL pathway's role in EMCV infection, we treated cells with the Arp2/3 complex inhibitor CK-869. CK-869 treatment inhibited EMCV infection in a dose-dependent manner without cell toxicity (Figure 6D and data not shown). Altogether, these data demonstrated that WASL and its downstream actin pathway play important roles in EMCV infection.

TNK2 is required for EMCV infection in an *in vivo* mouse model

337 To investigate TNK2's role in EMCV infection *in vivo*, we generated a TNK2 knockout mouse that
338 carried a 13Kb deletion of the murine TNK2 genomic locus, which eliminated all annotated TNK2
339 isoforms and splice variants (Figure 7A). In primary mouse lung fibroblast cells, complete ablation of
340 TNK2 protein expression was observed by Western blot (Figure 7B). The number of cells infected by
341 EMCV was reduced by 40% in the knockout cells ($P<0.001$, Figure 7C). *In vivo*, EMCV challenge with 10^7
342 PFU by oral gavage resulted in greater survival of TNK2 knockout animals compared to wild type animals
343 ($P=0.0051$, Figure 7D). Together, these data demonstrate a critical role for TNK2 in EMCV infection in an
344 *in vivo* mouse infection model.

345

346 **Discussion**

347 We previously determined that the *C. elegans* genes *sid-3*, *viro-2,* and *nck-1* are essential for
348 Orsay virus infection in *C. elegans* (10). In this study, we further asked whether their respective human
349 orthologues TNK2, WASL, and NCK1 play any roles in mammalian virus infection. After screening a panel
350 of mammalian viruses, we found that multiple picornaviruses, including EMCV, CVB3, enterovirus D68,
351 and poliovirus, rely on TNK2, WASL, and NCK1 for infection in different cell lines. For TNK2, this
352 represents the first evidence that it has any pro-viral function. Interestingly, poliovirus entry was
353 previously shown to be dependent on an unknown kinase based on the use of a broad-spectrum
354 tyrosine kinase inhibitor (4). One possibility is that TNK2 might be the kinase targeted in that study.

355 Our data represent the first demonstration that WASL and NCK1 are important for infection by
356 picornaviruses such as EMCV, CVB3, enterovirus D68, and poliovirus. RNA transfection of EMCV into
357 TNK2, WASL and NCK1 knockouts each yielded the same level of virus as the control demonstrating their
358 role in an early stage of the EMCV lifecycle. For WASL, this is in contrast to its well-defined role in
359 facilitating spread and transmission of vaccinia virus (22) suggesting that WASL is important for different

lifecycle stages for different viruses. In addition to the known interactions between NCK1 and WASL, TNK2 has been reported to phosphorylate WASL (15). Consistent with these data, our genetic epistasis analysis and ectopic trans-complementation data (Figure 3A-D) demonstrated that these three genes function in a pathway in the context of picornavirus infection. Furthermore, biochemical and biophysical data demonstrated direct interaction of NCK1 with both TNK2 and WASL. Previous studies have established a clear role for CDC42 in regulation of TNK2 and WASL (47, 50), inhibition of CDC42 resulted in reduced EMCV infection.

We explored the mechanism by which TNK2 and WASL act regarding picornavirus infection. TNK2 KO1 cells were partially defective in EMCV internalization. In contrast, internalization was not affected in WASL KO cells, suggesting WASL functions in one or more steps downstream of virus internalization. In the absence of either TNK2 or WASL, EMCV particles continued to accumulate in early endosomes at 30 minutes post infection in contrast to control cells, demonstrating a role for both genes in endosomal trafficking. Notably, *sid-3*, the *C. elegans* orthologue of TNK2, is important for endosomal trafficking of RNA molecules (51). Thus, one possibility is that the delay in release from the early endosomes contributes to the reduction in EMCV infection in both TNK2 and WASL KO cells. However, it is uncertain whether this observed accumulation in early endosomes is directly related to the reduced levels of infection in these cells. In detailed studies of poliovirus, most of the RNA genome is released from the virus particles by 20 minutes post internalization (4). Thus, additional studies are necessary to determine whether the accumulated particles in the early endosomes still contain genomic RNA.

These data lead us to the following model (Figure 8). TNK2 is in a pathway upstream of WASL and NCK1. Because TNK2 deletion has a greater magnitude of impact than WASL or NCK1 deletion, TNK2 must act on one or more additional step of the viral lifecycle than WASL and NCK1. Consistent with this model, we demonstrated that TNK2 (but not WASL) is needed for virus internalization. In addition, we

propose that TNK2 activates WASL (presumably, but not necessarily, by phosphorylation and in a fashion mediated by NCK1 binding), which then affects a subsequent early step of the EMCV lifecycle. Our data suggest that this step is linked to proper endocytic trafficking of the incoming viral particles, which accumulated in early endosomes in both TNK2 and WASL deficient cells to a greater extent than in control cells. The requirement for the WASL acidic domain, which is responsible for actin binding and nucleation, along with the sensitivity to the Arp2/3 inhibitor CK-869, demonstrates that this process is actin dependent. One possibility is that regulated actin polymerization may be necessary to deliver endocytic vesicles to specific subcellular locations necessary for productive infection.

Actin is critical for many cellular processes and due to its essentiality is not a druggable target. In this study, we identified a TNK2 and actin-dependent pathway necessary to promote virus infection but does not appear to alter normal endocytosis. As cells lacking TNK2 and NCK1 are clearly viable, as are mice lacking TNK2 and NCK1 (52), these genes are potential antiviral targets that could be disrupted by small molecules without compromising overall actin biology and survival of the host.

It is becoming increasingly clear that there are additional, poorly defined stages of the picornavirus lifecycle. A recent genetic screen identified PLA2G16 as an essential gene required for an early stage of multiple picornaviruses at a step post binding, internalization, and pore formation (40). Our study similarly suggests that WASL also acts after these stages. Further study is needed to determine whether WASL acts at the same stage as PLA2G16 or at a distinct step.

All four picornaviruses we tested were dependent on TNK2 and WASL. In contrast, viruses in other families such as influenza A virus, parainfluenza 5 and adenovirus 5 were not affected by absence of these genes, suggesting that picornaviruses may specifically depend on these host factors. PIV5 is known to enter cells by direct fusion at the cellular membrane and is not believed to utilize endocytic vesicles (39). The observed lack of dependence of PIV5 on TNK2 or WASL is consistent with a potential

406 role of TNK2 and WASL in modulating endocytic vesicle trafficking. In contrast, picornaviruses such as
407 poliovirus, CVB3 and EMCV are generally thought to utilize clathrin independent endocytic vesicles for
408 entry (5), while influenza A virus and adenovirus mostly rely on clathrin mediated endocytosis for their
409 entry (2). The magnitude of the phenotypes did vary significantly among the tested picornaviruses,
410 which is not surprising given the significant degree of divergence between these virus genomes and
411 differences in their entry requirements. Nonetheless all four tested picornaviruses displayed different
412 degree of dependence on this pathway. It will be important to test a wider range of picornaviruses to
413 determine exactly which taxa within the *Picornaviridae* are most reliant on these genes. It will also be of
414 great interest to test additional viruses from other families. The data suggesting a role of WASL in Lassa
415 virus infection (24) supports the notion that at least some viruses in other virus families may also
416 depend on one or more of these genes for infection.

417 In recent years, multiple studies of host factors critical for picornavirus infection have utilized
418 haploid gene-trap screening or CRISPR screening in mammalian cell lines (40, 53, 54). These studies
419 have identified multiple host genes required broadly for picornaviruses (40), as well as examples of
420 genes required for specific picornaviruses. For instance, ADAM9 was discovered as a potential receptor
421 for EMCV by CRISPR screening (54). Notably, the genes that we identified by starting with the *C. elegans*
422 Orsay virus genetic screen, TNK2, WASL, and NCK1, were not identified as hits in any of the direct
423 mammalian screens undertaken by others (40, 53, 54). Thus, these approaches provide complementary
424 experimental strategies that, ideally in the long run, will lead to comprehensive understanding of host
425 factors necessary for virus infection.

426 Our study of TNK2 was driven by our identification in *C. elegans* of *sid-3* as a host factor required
427 for Orsay virus infection (10). *sid-3* was originally identified in a genetic screen for mutants defective in
428 systemic spread of RNAi (51). That screening strategy also identified another *C. elegans* gene, *sid-1*, that

is reported to transport dsRNA (55). A recent study demonstrated that the mammalian orthologue of *sid-1*, SIDT2, has an evolutionarily conserved function in transporting dsRNA that serves as a means of activating innate antiviral immunity in mice (56). Those studies provide an example of the value of using the *C. elegans* model system to guide insights into conserved functions with mammals. Here we demonstrated that TNK2, the human orthologue of *sid-3*, has an evolutionarily conserved function to facilitate virus infection in mammals. In *C. elegans*, Orsay virus infection is presumed to occur by fecal-oral transmission, as evidenced by its exclusive intestinal cell tropism (57). Deletion of *sid-3* reduces Orsay virus infection by > 5 logs *in vivo* in the *C. elegans* host (10). In the current study, infection of mice lacking TNK2 by oral gavage, the analogous route of infection as for Orsay virus infection of *C elegans*, led to increased survival of animals deficient in TNK2. These results clearly demonstrate the functional parallels between *sid-3* and TNK2 in their respective hosts *in vivo*. Thus, our study has identified another example wherein novel insight in mammalian biology emerge from initial discoveries in model organism studies.

Material and methods

Cell culture and viruses

A549 cells were cultured and maintained in DMEM supplemented with 25 mM HEPES, 2 mM L-glutamine, 1X non-essential amino acids, 10% Fetal bovine serum (FBS) and 100 u/ml antibiotics (penicillin and streptomycin). 293T (human embryonic kidney), BHK-21 (Baby hamster kidney), RD (rhabdomyosarcoma) and Hela cells were cultured and maintained in DMEM with 10% FBS. Haploid cells (HAP1) were cultured and maintained in IMDM with 10% FBS. Mouse primary lung fibroblasts were isolated by lung digestion as described (58). Primary lung fibroblasts were derived from a TNK2 homozygous knockout mouse and a homozygous wild type littermate and were cultured in DMEM with

20% FBS. Viruses were obtained from the following: EMCV VR-129 strain (Michael Diamond), coxsackie virus B3 Nancy strain (Julie Pfeiffer), poliovirus Mahoney strain (Nihal Altan-Bonnet), influenza A virus WSN strain (H1N1) (Adrianus Boon), adenovirus A5 (David Curiel), enterovirus D68 (ATCC), parainfluenza virus (Robert A. Lamb), GFP-EMCV and GFP-CVB3 (Frank J. M. van Kuppeveld). EMCV was amplified on BHK-21 cells; CVB3 and polio viruses were amplified on HeLa cells; and enterovirus D68 was amplified on RD cells.

Reagents and antibodies

α-sarcin was purchased from Santa Cruz. ^{35}S methionine and ^{35}S cysteine were purchased from Perkin Elmer. Alexa Fluor^{TM}A647 succinimidyl ester was purchased from ThermoFisher Scientific. Inhibitors were purchased from commercial vendors as follow: Aim-100 (Apexbio), Wiskostatin (Sigma), Dynasore (Sigma), Pitstop-2 (Sigma), CK-869 (Sigma), Pirl1 (Hit2leads). Anti-EMCV mouse polyclonal antibodies were provided by Michael Diamond. Anti-poliovirus antibodies were provided by Nihal Altan-Bonnet. Other antibodies were obtained from commercial vendors as follows: Anti-coxsackie virus B3 antibodies (ThermoFisher), Anti-adenovirus A5 antibodies (ThermoFisher), Anti-influenza A virus NP antibodies (Millipore), Anti-TNK2 (A12) (Santa Cruz), Anti-WASL (Abcam and Sigma), Anti-actin, clone C4 (Sigma), Anti-NCK1 (Millipore), enterovirus D68 Ab (GeneTex), Anti-HA (ThermoFisher), Anti-Flag (GenScript), Anti-c-Myc (Invitrogen), Anti-double stranded J2 antibodies (Scicons).

Plasmid constructions

Single guide RNA (sgRNA) oligonucleotides were synthesized by Integrated DNA Technologies (IDT). sgRNA oligoes were annealed and cloned into Lenti-CRISPR V2 plasmid digested by BsmBI. TNK2 (pReceiver-TNK2) and WASL (pReceiver-WASL) ORF clones were obtained from GeneCopoeia. NCK1 (pcDNA-NCK1) ORF clone was obtained from GenScript. Mutations in the sgRNA binding sites were introduced by site directed mutagenesis (Stratagene) according to the manufacturer's protocol. TNK2,

475 WASL and NCK1 were subcloned into a Lentivirus expression vector pFCIV digested with Asc1 and Age1.
476 The FRET control plasmid C5V was obtained from Addgene. mVenus cassette was subcloned into
477 pcDNA-NCK1 and pReceiver-WASL. mCerulean cassette was subcloned into pReceiver-TNK2. Myc tagged
478 TNK2 and HA tagged WASL was generated by annealing of oligonucleotides and then subcloned into the
479 expression vector. GFP tagged TNK2 and WASL were subcloned into a tetracycline promoter driven
480 Lentivirus vector pCW57. Constitutive active WASL constructs were generated by site-directed
481 mutagenesis. Domain truncation were generated by overlapping PCR. In brief, to generate pFCIV-WASL
482 Δ WH1, pFCIV-WASL Δ B, pFCIV-WASL Δ PRD, pFCIV-WASL Δ GBD, and pFCIV-WASL Δ A, WASL
483 fragments were amplified from the start of the gene to the start of the truncation and from the end of
484 the truncation to the end of the gene, and the fragments were then joined by overlapping PCR. The
485 resulting product was digested by AgeI and AscI and ligated into Lentivirus expression vector pFCIV that
486 were cut by the same restriction enzymes.

487 Lentivirus production and cell transduction

488 800 ng of Lenti CRISPR V2 plasmids or pFCIV plasmids or pCW57 plasmids were transfected with 800 ng
489 pSPAX2 and 400 ng pMD2.G into 293T cells using Lipofectamine 2000 according to the manufacturer's
490 protocol. Cell culture supernatant was harvested two days post transfection and stored at -80°C. For
491 transduction, A549 cells were seeded one day before transduction. Cells were spin transfected with
492 lentivirus and 8 μg/ml of polybrene at MOI 5. Two days after transduction, cells were passaged and
493 either selected under corresponding antibiotics or fluorescently sorted through flow cytometry.

494 CRISPR genome editing

495 A549 naïve cells were transduced by lentiviruses that express the corresponding sgRNA and Cas9 protein.
496 Transduced cells were passaged two days later and then selected with 2 μg/ml puromycin for 7 days.
497 Cells were passaged once during this selection. Clonal selection was performed through limiting dilution

498 in 96-well plates. After two weeks, single cell clones were picked and expanded in 24-well plates. The
499 desired genome editing was identified by a restriction enzyme digestion-based genome typing assay.
500 Genome edited clonal cells were further sequenced by Sanger sequencing to define the precise genome
501 editing event. Detection of a homozygous 28bp (base pair) deletion allele of TNK2 defined TNK2 KO1
502 and detection of a 25bp deletion allele and 137bp deletion allele of TNK2 defined TNK2 KO2.
503 Identification of a 1bp insertion allele and a 2 bp deletion allele of WASL defined WASL KO. An insertion
504 allele of 94 bp in NCK1 was observed and this defined NCK1 KO. TNK2 KO1, WASL KO and NCK1 KO were
505 used in all experiments except places specified using other cells.

506 For homologous template directed DNA repair through CRISPR genome editing, assembled CRISPR RNP
507 were transfected into A549 cells with single stranded oligodeoxynucleotide (ssODN) as described (59). In
508 brief, Alt-R® S.p. Cas9 nuclease 3NLS protein, Alt-R® CRISPR-Cas9 crRNA designed to target the deleted
509 TNK2 KO1 genomic region, Alt-R® CRISPR-Cas9 ATTO™ 550 tagged tracrRNA and ssODN were purchased
510 from IDT. A549 cells were seeded into 12-well plates one day before transfection. Equal molar crRNA
511 and tracrRNA were annealed by heating to 95 °C for 5 minutes and then cooled to room temperature.
512 RNP was assembled by combing equal molar ratio of annealed cr-tracrRNA with Cas9 nuclease protein in
513 opti-MEM. RNP was then transfected with ssODN into A549 cells by lipofectamine CRISPR-MAX
514 according to the manufacturer's protocol. 24 hours after transfection, ATTO™ 550 positive cells were
515 FACS sorted individually into 96-well plates. Single cell colonies were expanded one week after sorting
516 and genotyped with a restriction enzyme based genotyping assay. Template directed DNA repair was
517 finally confirmed by both Sanger and PCR product deep sequencing.

518 For generation of gene double or triple knockout cells, the same CRISPR RNP transfection method was
519 used as homologous template directed DNA repair using corresponding crRNA designed to target genes
520 with ssODN omitted. A double knockout of NCK1 and WASL was generated by CRISPR-Cas9 genome

editing of the NCK1 locus in the WASL KO cells. A double knockout of WASL and TNK2, a double knockout of NCK1 and TNK2, and a triple knockout of WASL, NCK1 and TNK2 were generated by CRISPR-Cas9 genome editing of the WASL locus and NCK1 locus in the TNK2 KO1 cells. Genome editing events were screened by a restriction enzyme digestion-based genotyping assay.

EMCV virus labeling and infection for imaging

EMCV was amplified in BHK-21 cells and purified according to previous publications (4, 40). Virus labeling was performed with Alexa Fluor™A647 succinimidyl ester in a 1:10 molar ratio and was then purified through Nap-5 desalting column (GE Healthcare). Labeled viruses were aliquoted and stored at -80°C. For EMCV entry imaging analysis, A549 cells were seeded at 3000 cells per well in an 18-well IBD imaging slide chamber one day before infection. The next day, cells were washed once with serum free DMEM and then inoculated with labeled EMCV virus at an MOI of 20 on ice for one hour. Cells were washed three times with ice-cold PBS after on ice binding. Cells were then fixed with 4% paraformaldehyde for 15 minutes at room temperature or cells were switched to 37°C incubation with complete medium for internalization. After incubation with complete medium for 30 minutes, cells were then washed once with PBS and fixed with 4% paraformaldehyde. Fixed cells were mounted in IBD mounting medium for image analysis. For GFP-TNK2 and GFP-WASL localization with labeled EMCV virus imaging, live cell experiment was performed in an 18-well IBD imaging slide in a temperature-controlled imaging chamber.

EMCV virus binding and internalization assay

A549 cells were seeded at $1X10^5$ cell per well in a 24-well plate one day before the assay. Cells were chilled on ice for 30 minutes and then washed with ice-cold DMEM before inoculation. EMCV was diluted in ice-cold DMEM with 0.1% BSA and then inoculated at an MOI of 20 in 250 μl of DMEM per well of 24-well plate. Viruses were allowed to bind on ice for one hour. For virus binding experiments,

cells were washed three times with ice-cold PBS and then lysed in 350 μl Trizol reagent. For virus internalization assay using trypsinization, experiments were performed as described previously for WNV and AAV (34, 35). In brief, after one hour of binding, the virus inoculum was removed and pre-warmed complete medium was added onto cells. Cells were incubated in a 37°C water bath for 30 minutes to allow for virus internalization. After incubation, cells were washed three times with ice-cold PBS and then trypsinized for 6 minutes to remove surface bound virus. Trypsinized cells were then washed again three times and then spin at 300g for 5 minutes. Cell pellets were lysed in 350 μl Trizol reagents. RNA was extracted using the 96-well Zymo RNA easy column extraction according to the manufacturer's protocol. Viral RNA was quantified by one step reverse transcription quantitative real-time PCR with an EMCV assay probe (Primers: forward 5'-CGATCACTATGCTTGCCGTT-3'; reverse 5'-CCCTACCTCACGGAATGGG-3'; Taqman probe 5' FAM-AGAGCCGATCATATTCCTGCTTGCCA-3'). Fold change was converted from delta delta Ct of an internal control assay by RPLP0 (Ribosomal protein lateral stalk subunit P0). For labeled EMCV, internalization was performed the same way, after trypsinization and washing, cells were fixed in 4% paraformaldehyde for 15 minutes at room temperature and then washed twice with P2F (PBS with 2% Fetal bovine serum). Cells were finally resuspended in P2F and analyzed by MACS flow cytometry.

FACS assay

A549 cells were seeded one day before infection into 96-well plates. Approximately 16 hours after seeding, cells were infected by EMCV at an MOI of 1. One hour after infection, the inoculum was removed and cells were cultured in DMEM with 2% FBS. 10 hours post infection, cells were trypsinized and fixed with 4% paraformaldehyde. Fixed cells were then permeabilized with perm buffer (1g Saponin, 10ml HEPES, 0.025% Sodium Azide in 1L HBSS) for 15 minutes. After permeabilization, cells were incubated with primary antibodies for one hour and then washed twice before incubation with

567 fluorescently conjugated secondary antibodies. After one hour of secondary antibody incubation, cells
568 were washed three times with perm buffer and then resuspended with 70 μl of FACS buffer P2F (PBS
569 with 2% fetal bovine serum). Infected cells were then analyzed and quantified through MACS flow
570 cytometry (Miltenyi Biotec). FACS analysis of infection by CVB3, polio, enterovirus D68, adenovirus and
571 influenza virus on either A549 or Hap1 cells were performed the same as EMCV infection, except that
572 cells were harvested 8 hours post infection for CVB3, adenovirus, enterovirus D68 and influenza virus,
573 and 6 hours post infection for poliovirus.

574 Multistep growth analysis for EMCV and polio virus

575 For multistep growth analysis, A549 or Hap1 cells were infected by EMCV at an MOI of 0.01. One hour
576 after inoculation, cells were washed 5 times with serum free DMEM and were then cultured in DMEM or
577 IMDM with 2% FBS. Culture supernatant was collected at time 0, 6, 12, 24, 36 and 48 hours post
578 infection. Viruses released in the culture supernatant were titrated on BHK-21 cells by plaque assay. For
579 polio virus multi-step growth titration, A549 or Hap1 cells were infected by virus at MOI 0.01 and culture
580 supernatant were collected. Released viruses were titrated on HeLa cells by plaque assay.

581 EMCV genomic RNA transfection

582 EMCV genomic RNA was extracted from pelleted virions by phenol chloroform extraction. For RNA
583 transfection, A549 cells (gene knockouts and control) were seeded into 24-well plate at $1X10^5$ cells per
584 well. 16 hours after seeding, cells were transfected with 1.6 μg EMCV RNA by Lipofectamine 3000
585 according to the manufacturer's protocol. Cell culture supernatant was collected at 10 hours post
586 transfection and was then titrated on BHK-21 cells by plaque assay.

587 Co-immunoprecipitation and Western blot

588 Flag C-terminal tagged NCK1 was transfected with HA N-terminal tagged WASL or with Myc N-terminal
589 tagged TNK2 into 293T cells. 48 hours after transfection, cells were lysed in IpLysis buffer (Invitrogen).
590 Protein concentrations were quantified by BCA assay. 500 μg protein lysates were incubated with 2 μg
591 of anti-flag antibodies at 4°C for overnight for immunoprecipitation. After antibody binding, the
592 immuno-complex was incubated with protein A/G magnetic beads for one hour at room temperature.
593 The beads were washed and proteins bound to antibodies were eluted according to the manufacture's
594 protocol (Invitrogen). Protein samples were prepared with 4X NuPAGE sample buffer (Invitrogen) and
595 then resolved on 4-12% NuPAGE gel. Proteins were transferred to a PVDF membrane and then blocked
596 with 5% skim milk. Primary antibodies were incubated in 5% milk for overnight at 4°C. After 3 washes
597 with PBST (PBS with 0.3% of tween-20), corresponding HRP conjugated secondary antibodies were
598 incubated in 5% milk at room temperature for 1 hour. The membrane was washed 5 times with PBST
599 and was then developed with chemiluminescent substrate for 5 minutes and then imaged using a Bio-
600 Rad chemiluminescence imager.

601 α-Sarcin pore forming assay

602 A549 cells were seeded at 3.6 X 10^4 per well of a 48-well plate. The next day, cells were washed once
603 with PBS and then incubated with methionine and cysteine free DMEM for one hour. Subsequently, cells
604 were inoculated with EMCV virus at an MOI of 50 on ice for one hour. Inoculum were then removed and
605 cells were washed three times with ice cold PBS. Cells were then incubated with 100 μg/ml α-sarcin
606 diluted in methionine and cysteine free DMEM for 90 minutes at 37°C. After α-sarcin treatment, cells
607 were pulsed with 7.4 MBq ^{35}S methionine and ^{35}S cysteine in DMEM for 20 minutes. Next, cells were
608 washed four times with ice cold PBS and then lysed with SDS sample buffer. Proteins were resolved on
609 7.5% SDS-PAGE gel and then dried on a Bio-Rad gel dryer. Dried gels were exposed to a phosphorimager
610 overnight and then scanned by Fuji IFA imaging system. As an internal loading control, a parallel SDS-

611 PAGE gel was ran and then proteins were transferred to PVDF membrane and blotted with anti-actin
612 antibodies.

613 Immunofluorescence assay

614 For EMCV co-localization with EEA1 marker, A549 cells were seeded at 3000 cells per well in an 18-well
615 IBD imaging slide chamber one day before infection. The next day, cells were washed once with serum
616 free DMEM and then inoculated with labeled EMCV virus at an MOI of 20 on ice for one hour. Cells were
617 washed three times with PBS after on ice binding. Cells were then switched to 37°C incubation with
618 complete medium for internalization at indicated time. After incubation with complete medium for
619 different time, cells were then washed once with PBS and fixed with 4% paraformaldehyde for 10
620 minutes. Fixed cells were then permeabilized with 0.2% saponin for 10 minutes at room temperature
621 and subsequently blocked with IFA blocking buffer (10% goat serum, 0.05% saponin in PBS) at room
622 temperature for 30 minutes. Cells were then incubated with EEA1 antibodies at 1:100 dilution in
623 blocking buffer overnight with shaking. Cells were washed three times with PBS and then incubated with
624 secondary antibodies at room temperature for 1 hour. After incubation, cells were washed once with
625 PBS and then incubated with Hoechst at 1:1000 dilution for 10 minutes at room temperature. Cells were
626 washed three time with PBS and mounted in IBD mounting medium for image analysis. For dsRNA
627 immunostaining in EMCV infected cells, the same procedure was performed as EEA1 immunostaining
628 except that 0.1% Triton was used instead of Saponin.

629 Confocal imaging and FRET analysis

630 Cells on slides or in an IBD imaging slide chamber were examined on a Zeiss airy scan confocal
631 microscope (LSM 880 II). A Plan Apochromat 63X, 1.4-numerical-aperture oil objective lens (Carl Zeiss,
632 Germany) was used to image labeled virus infection. For FRET analysis, 293T cells were seeded on
633 coverslips and transfected with FRET pairs, mCerluean tagged TNK2 with mVenus tagged NCK1 and

mCerulean tagged WASL with mVenus tagged NCK1 respectively. 24 hours post transfection, cells were fixed in 4% paraformaldehyde and mounted on slides. Cells were imaged on a Zeiss airy scan confocal with a Plan Apochromat 100X, 1.4-numerical-aperture oil objective lens. Acceptor photo bleach was performed with 80% laser intensity of the imaging channel. Images were taken before and after photo bleach and FRET efficiency were calculated after image acquisition on Zen pro software (Carl Zeiss, Germany). For quantification of EMCV colocalization with EEA1, image analysis was performed using Volocity software V6.3 (PerkinElmer).

Transmission electron microscopy

EMCV was incubated with A549 cells (wild type, TNK2 KO and WASL KO) at an MOI of 20 for 1 hour on ice. Cells were then washed with serum free DMEM and incubated with A549 culture media (2% FBS) for 6 hours. Infected cells were washed with PBS and fixed with 2% paraformaldehyde, 2.5% glutaraldehyde (Polysciences Inc., Warrington, PA) in 100 mM cacodylate buffer for 1 hour at room temperature. Next, cells were scraped from plates using a rubber cell scraper and cell pellets were embedded in agarose. Agarose embedded cell pellets were post-fixed in 1% osmium tetroxide (Polysciences Inc.) for 1 hour, then rinsed extensively in dH20 prior to *en bloc* staining with 1% aqueous uranyl acetate (Ted Pella Inc., Redding, CA) for 1 hour. Following several rinses in dH20, samples were dehydrated in a graded series of ethanol and embedded in Eponate 12 resin (Ted Pella Inc.). Sections of 95 nm were cut with a Leica Ultracut UCT ultramicrotome (Leica Microsystems Inc., Bannockburn, IL), stained with uranyl acetate and lead citrate, and viewed on a JEOL 1200EX transmission electron microscope (JEOL USA, Peabody, MA) equipped with an AMT 8 mega-pixel digital camera (Advanced Microscopy Techniques, Woburn, MA).

In vivo infection experiments

Animal experiments were conducted under the supervision of Department of Comparative Medicine at Washington University in St. Louis. All animal protocols were approved by the Washington University Institutional Animal Care and Use Committee (Protocol #20170194 and #20180289). TNK2 knockout mice were generated in the C57BL/6 background by CRISPR-Cas9 genome editing at the Genome Engineering and iPSC Center (GEiC) at Washington University. All animals were housed in the pathogen free barrier. Age-matched animals with mixed gender (6-8 weeks old, 5 females and 6 males for TNK2 knockout, 2 females and 5 males for wild type littermates) were infected with $1X10^7$ PFU of EMCV (two doses at day 0 and day 1) via oral gavage according to previous publication (60). Infected mice were monitored for at least 10 days for all experiments.

Statistical analysis

For statistical analysis, Student T-test was performed on the average values from three replicates. All data shown with statistics are representative of at least two independent experiments. Log-rank test was done in Graphpad Prism V7. Statistical significance are indicated as below: NS: no statistical significance, *: P<0.05, **: P<0.01, ***: P<0.001, ****: P<0.0001, *****: P<0.00001.

Acknowledgement

This work was supported in part by National Institutes of Health R01 AI134967.

We thank Adrianus Boon, Skip Virgin, Celeste Morley and John Cooper for helpful discussions. We thank Rong Zhang and Michael S. Diamond for access to FACS instrumentation. FRET experiments were performed at the Washington University Center for Cellular Imaging (WUCCI) supported by Washington University School of Medicine, The Children's Discovery Institute of Washington University and St. Louis Children's Hospital (CDI-CORE-2015-505) and the Foundation for Barnes-Jewish Hospital (3770). We

678 thank Wandy Beatty for assistance with electron microscopy and laser scanning confocal. We thank the
679 Genome Engineering and iPSC Center (GEiC) at the Washington University in St. Louis for their sgRNA
680 validation and genotyping services for generating the TNK2 knockout mouse. We thank the flow
681 cytometry core at Department of Pathology and Immunology, Washington University School of Medicine
682 for assisting cell sorting. We thank Tim Schaff and Darren Kreamalmeyer for assistance with mouse
683 breeding.

684

685 **Author Contributions**

686 H.J. performed the *in vitro* and *in vivo* experiments, including the primary CRISPR/Cas9 knockout of
687 TNK2, WASL, validation in different cells with different viruses, gene rescue, RNA genome transfection,
688 virus binding, internalization, pore-formation, host factor cleavage, FRET, co-immunoprecipitation, co-
689 localization assays, *etc*. C.L. generated expression clones, part of the double knockout clones, performed
690 the constitutive WASL rescue, domain analysis of WASL, and generated figure 3A-D and figure 6A-C. S.T.
691 generated NCK1 KO cells, conducted the experiments in figure 2F-H, and performed quantitative image
692 analysis. H. J. and D. W. designed the experiments and performed data analysis. H.J. wrote the initial
693 draft of the manuscript, with D. W. editing and the other authors contributing to the final paper.

694

695 **Declaration of Interests**

696 The authors declare no competing interests.

697 **References**

698 1. Melnick JL (1983) Portraits of viruses: the picornaviruses. *Intervirology* 20(2-3):61-100.
699 2. Yamauchi Y & Helenius A (2013) Virus entry at a glance. *J Cell Sci* 126(Pt 6):1289-1295.

3. Madshus IH, Olsnes S, & Sandvig K (1984) Requirements for entry of poliovirus RNA into cells at low pH. *The EMBO journal* 3(9):1945-1950.
4. Brandenburg B*, et al.* (2007) Imaging poliovirus entry in live cells. *PLoS biology* 5(7):e183.
5. Bergelson JM & Coyne CB (2013) Picornavirus entry. *Advances in experimental medicine and biology* 790:24-41.
6. Coyne CB & Bergelson JM (2006) Virus-induced Abl and Fyn kinase signals permit coxsackievirus entry through epithelial tight junctions. *Cell* 124(1):119-131.
7. Coyne CB, Shen L, Turner JR, & Bergelson JM (2007) Coxsackievirus entry across epithelial tight junctions requires occludin and the small GTPases Rab34 and Rab5. *Cell host & microbe* 2(3):181-192.
8. Huber SA (1994) VCAM-1 is a receptor for encephalomyocarditis virus on murine vascular endothelial cells. *Journal of virology* 68(6):3453-3458.
9. Madshus IH, Olsnes S, & Sandvig K (1984) Different pH requirements for entry of the two picornaviruses, human rhinovirus 2 and murine encephalomyocarditis virus. *Virology* 139(2):346-357.
10. Jiang H, Chen K, Sandoval LE, Leung C, & Wang D (2017) An Evolutionarily Conserved Pathway Essential for Orsay Virus Infection of Caenorhabditis elegans. *mBio* 8(5).
11. Galisteo ML, Yang Y, Urena J, & Schlessinger J (2006) Activation of the nonreceptor protein tyrosine kinase Ack by multiple extracellular stimuli. *Proceedings of the National Academy of Sciences of the United States of America* 103(26):9796-9801.
12. Donnelly SK, Weisswange I, Zettl M, & Way M (2013) WIP provides an essential link between Nck and N-WASP during Arp2/3-dependent actin polymerization. *Current biology : CB* 23(11):999-1006.
13. Liu Y*, et al.* (2010) Dasatinib inhibits site-specific tyrosine phosphorylation of androgen receptor by Ack1 and Src kinases. *Oncogene* 29(22):3208-3216.
14. Mahajan NP, Whang YE, Mohler JL, & Earp HS (2005) Activated tyrosine kinase Ack1 promotes prostate tumorigenesis: role of Ack1 in polyubiquitination of tumor suppressor Wwox. *Cancer Res* 65(22):10514-10523.
15. Yokoyama N, Lougheed J, & Miller WT (2005) Phosphorylation of WASP by the Cdc42-associated kinase ACK1: dual hydroxyamino acid specificity in a tyrosine kinase. *The Journal of biological chemistry* 280(51):42219-42226.
16. Fujimoto Y*, et al.* (2011) A single nucleotide polymorphism in activated Cdc42 associated tyrosine kinase 1 influences the interferon therapy in hepatitis C patients. *Journal of hepatology* 54(4):629-639.
17. Konig R*, et al.* (2010) Human host factors required for influenza virus replication. *Nature* 463(7282):813-817.
18. Karlas A*, et al.* (2010) Genome-wide RNAi screen identifies human host factors crucial for influenza virus replication. *Nature* 463(7282):818-822.
19. Lupberger J*, et al.* (2011) EGFR and EphA2 are host factors for hepatitis C virus entry and possible targets for antiviral therapy. *Nature medicine* 17(5):589-595.
20. Massaad MJ, Ramesh N, & Geha RS (2013) Wiskott-Aldrich syndrome: a comprehensive review. *Annals of the New York Academy of Sciences* 1285:26-43.
21. Teo M, Tan L, Lim L, & Manser E (2001) The tyrosine kinase ACK1 associates with clathrin-coated vesicles through a binding motif shared by arrestin and other adaptors. *The Journal of biological chemistry* 276(21):18392-18398.
22. Frischknecht F*, et al.* (1999) Actin-based motility of vaccinia virus mimics receptor tyrosine kinase signalling. *Nature* 401(6756):926-929.

23. Dodding MP & Way M (2009) Nck- and N-WASP-dependent actin-based motility is conserved in divergent vertebrate poxviruses. *Cell host & microbe* 6(6):536-550.
24. Oppliger J, Torriani G, Herrador A, & Kunz S (2016) Lassa Virus Cell Entry via Dystroglycan Involves an Unusual Pathway of Macropinocytosis. *Journal of virology* 90(14):6412-6429.
25. Wolf YI*, et al.* (2018) Origins and Evolution of the Global RNA Virome. *mBio* 9(6).
26. Zerbino DR*, et al.* (2018) Ensembl 2018. *Nucleic acids research* 46(D1):D754-D761.
27. Mahajan K*, et al.* (2010) Effect of Ack1 tyrosine kinase inhibitor on ligand-independent androgen receptor activity. *The Prostate* 70(12):1274-1285.
28. Peterson JR*, et al.* (2004) Chemical inhibition of N-WASP by stabilization of a native autoinhibited conformation. *Nature structural & molecular biology* 11(8):747-755.
29. Yokoyama N & Miller WT (2003) Biochemical properties of the Cdc42-associated tyrosine kinase ACK1. Substrate specificity, authphosphorylation, and interaction with Hck. *J Biol Chem* 278(48):47713-47723.
30. Adamovich DA*, et al.* (2009) Activating mutations of N-WASP alter Shigella pathogenesis. *Biochemical and biophysical research communications* 384(3):284-289.
31. Keszei M*, et al.* (2018) Constitutive activation of WASp in X-linked neutropenia renders neutrophils hyperactive. *The Journal of clinical investigation* 128(9):4115-4131.
32. Rohatgi R, Nollau P, Ho HY, Kirschner MW, & Mayer BJ (2001) Nck and phosphatidylinositol 4,5-bisphosphate synergistically activate actin polymerization through the N-WASP-Arp2/3 pathway. *The Journal of biological chemistry* 276(28):26448-26452.
33. Shen H*, et al.* (2011) Constitutive activated Cdc42-associated kinase (Ack) phosphorylation at arrested endocytic clathrin-coated pits of cells that lack dynamin. *Molecular biology of the cell* 22(4):493-502.
34. Berry GE & Tse LV (2017) Virus Binding and Internalization Assay for Adeno-associated Virus. *Bio Protoc* 7(2).
35. Hackett BA*, et al.* (2015) RNASEK is required for internalization of diverse acid-dependent viruses. *Proceedings of the National Academy of Sciences of the United States of America* 112(25):7797-7802.
36. Grovdal LM, Johannessen LE, Rodland MS, Madshus IH, & Stang E (2008) Dysregulation of Ack1 inhibits down-regulation of the EGF receptor. *Experimental cell research* 314(6):1292-1300.
37. Innocenti M*, et al.* (2005) Abi1 regulates the activity of N-WASP and WAVE in distinct actin-based processes. *Nature cell biology* 7(10):969-976.
38. Fernandez-Puentes C & Carrasco L (1980) Viral infection permeabilizes mammalian cells to protein toxins. *Cell* 20(3):769-775.
39. Porotto M, Palmer SG, Palermo LM, & Moscona A (2012) Mechanism of fusion triggering by human parainfluenza virus type III: communication between viral glycoproteins during entry. *The Journal of biological chemistry* 287(1):778-793.
40. Staring J*, et al.* (2017) PLA2G16 represents a switch between entry and clearance of Picornaviridae. *Nature* 541(7637):412-416.
41. Glaser W & Skern T (2000) Extremely efficient cleavage of eIF4G by picornaviral proteinases L and 2A in vitro. *FEBS Lett* 480(2-3):151-155.
42. Carthy CM*, et al.* (1998) Caspase activation and specific cleavage of substrates after coxsackievirus B3-induced cytopathic effect in HeLa cells. *Journal of virology* 72(9):7669-7675.
43. Jones S, Cunningham DL, Rappoport JZ, & Heath JK (2014) The non-receptor tyrosine kinase Ack1 regulates the fate of activated EGFR by inducing trafficking to the p62/NBR1 pre-autophagosome. *J Cell Sci* 127(Pt 5):994-1006.
44. Prieto-Echague V, Gucwa A, Brown DA, & Miller WT (2010) Regulation of Ack1 localization and activity by the amino-terminal SAM domain. *BMC Biochem* 11:42.

45. Howlin J, Rosenkvist J, & Andersson T (2008) TNK2 preserves epidermal growth factor receptor expression on the cell surface and enhances migration and invasion of human breast cancer cells. *Breast cancer research : BCR* 10(2):R36.
46. Mahajan NP*, et al.* (2007) Activated Cdc42-associated kinase Ack1 promotes prostate cancer progression via androgen receptor tyrosine phosphorylation. *Proceedings of the National Academy of Sciences of the United States of America* 104(20):8438-8443.
47. Rohatgi R, Ho HY, & Kirschner MW (2000) Mechanism of N-WASP activation by CDC42 and phosphatidylinositol 4, 5-bisphosphate. *The Journal of cell biology* 150(6):1299-1310.
48. Galletta BJ, Chuang DY, & Cooper JA (2008) Distinct roles for Arp2/3 regulators in actin assembly and endocytosis. *PLoS biology* 6(1):e1.
49. Stradal TE*, et al.* (2004) Regulation of actin dynamics by WASP and WAVE family proteins. *Trends in cell biology* 14(6):303-311.
50. Prieto-Echague V & Miller WT (2011) Regulation of ack-family nonreceptor tyrosine kinases. *Journal of signal transduction* 2011:742372.
51. Jose AM, Kim YA, Leal-Ekman S, & Hunter CP (2012) Conserved tyrosine kinase promotes the import of silencing RNA into Caenorhabditis elegans cells. *Proceedings of the National Academy of Sciences of the United States of America* 109(36):14520-14525.
52. Bladt F*, et al.* (2003) The murine Nck SH2/SH3 adaptors are important for the development of mesoderm-derived embryonic structures and for regulating the cellular actin network. *Molecular and cellular biology* 23(13):4586-4597.
53. Kim HS*, et al.* (2017) CRISPR/Cas9-mediated gene knockout screens and target identification via whole-genome sequencing uncover host genes required for picornavirus infection. *The Journal of biological chemistry* 292(25):10664-10671.
54. Bazzone LE*, et al.* (2019) A Disintegrin and Metalloproteinase 9 Domain (ADAM9) Is a Major Susceptibility Factor in the Early Stages of Encephalomyocarditis Virus Infection. *mBio* 10(1).
55. Winston WM, Molodowitch C, & Hunter CP (2002) Systemic RNAi in C. elegans requires the putative transmembrane protein SID-1. *Science* 295(5564):2456-2459.
56. Nguyen TA*, et al.* (2017) SIDT2 Transports Extracellular dsRNA into the Cytoplasm for Innate Immune Recognition. *Immunity* 47(3):498-509 e496.
57. Franz CJ*, et al.* (2014) Orsay, Santeuil and Le Blanc viruses primarily infect intestinal cells in Caenorhabditis nematodes. *Virology* 448:255-264.
58. Edelman BL & Redente EF (2018) Isolation and Characterization of Mouse Fibroblasts. *Methods Mol Biol* 1809:59-67.
59. Jacobi AM*, et al.* (2017) Simplified CRISPR tools for efficient genome editing and streamlined protocols for their delivery into mammalian cells and mouse zygotes. *Methods* 121-122:16-28.
60. Wang P*, et al.* (2015) Nlrp6 regulates intestinal antiviral innate immunity. *Science* 350(6262):826-830.

Figure 1

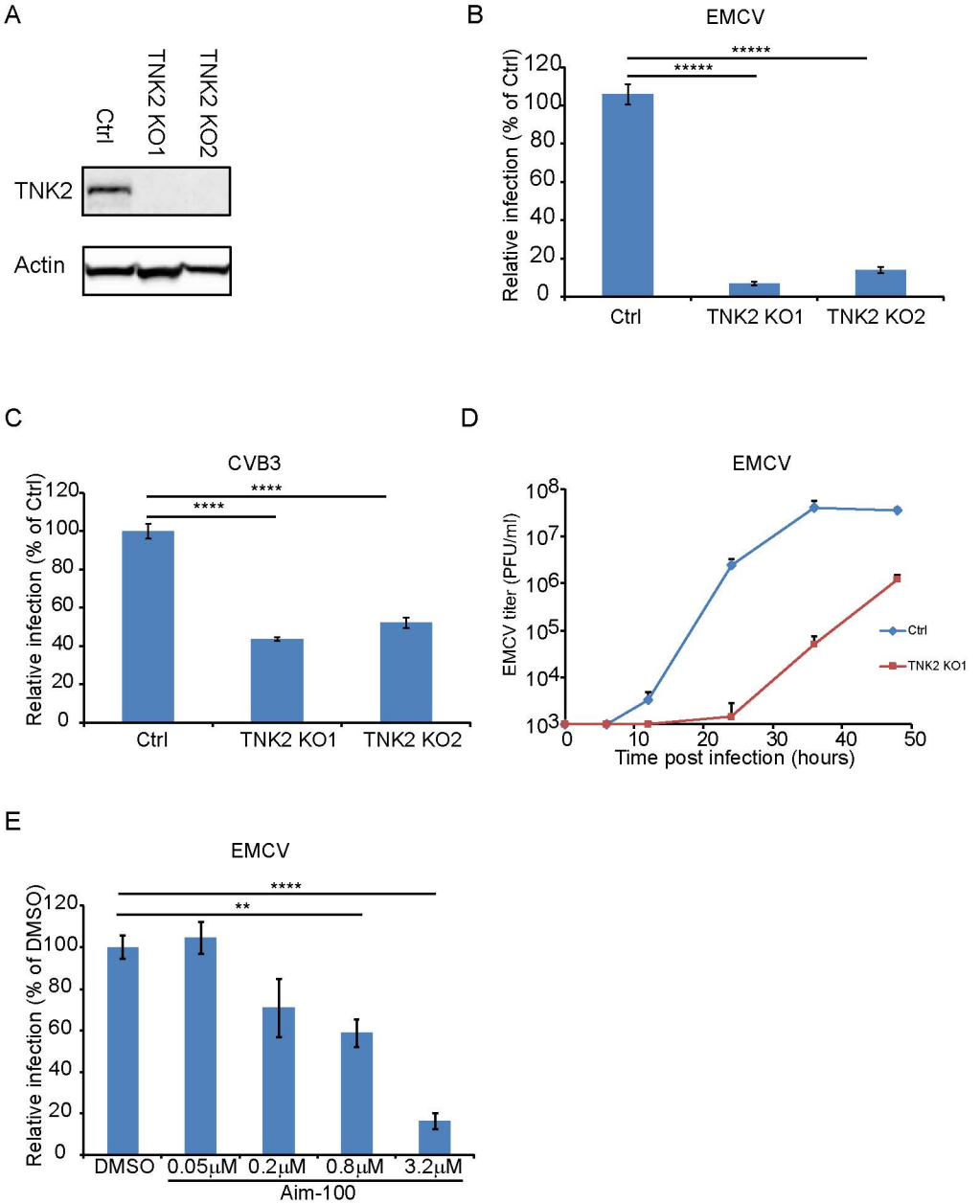

Figure 1. TNK2 is critical for multiple picornavirus infections.
(A) TNK2 protein expression in TNK2 KO1, TNK2 KO2 and Ctrl (control) cells generated by CRISPR-Cas9 genome editing with either specific targeting or non-specific targeting sgRNA in A549 cells. Cells lysates were analyzed by Western blot.
(B) FACS quantification of EMCV positive cells for TNK2 KO1, TNK2 KO2, and Ctrl cells 10 hours post infection at an MOI of 1.
(C) FACS quantification of CVB3 virus positive cells for TNK2 KO1, TNK2 KO2, and Ctrl cells 8 hours post infection at an MOI of 1.
(D) Multi-step growth curve for EMCV multiplication on TNK2 KO1 and Ctrl cells at an MOI of 0.01. Virus titers in the culture super-natant were quantified by plaque assay at 0, 6, 12, 24, 36, and 48 hours post infection.
(E) Aim-100 inhibition of EMCV infection on naïve A549 cells. A549 cells were pre-treated with Aim-100 at indicated concentrations and infected with EMCV at an MOI of 1. Virus positive cells were quantified by FACS.
(B-E) Error bars represent standard deviation of three replicates. The data shown are representatives of three independent experiments.
*: P<0.05, ***: P<0.001, ****: P<0.0001, *****: P<0.00001.

Figure 1-figure supplement1

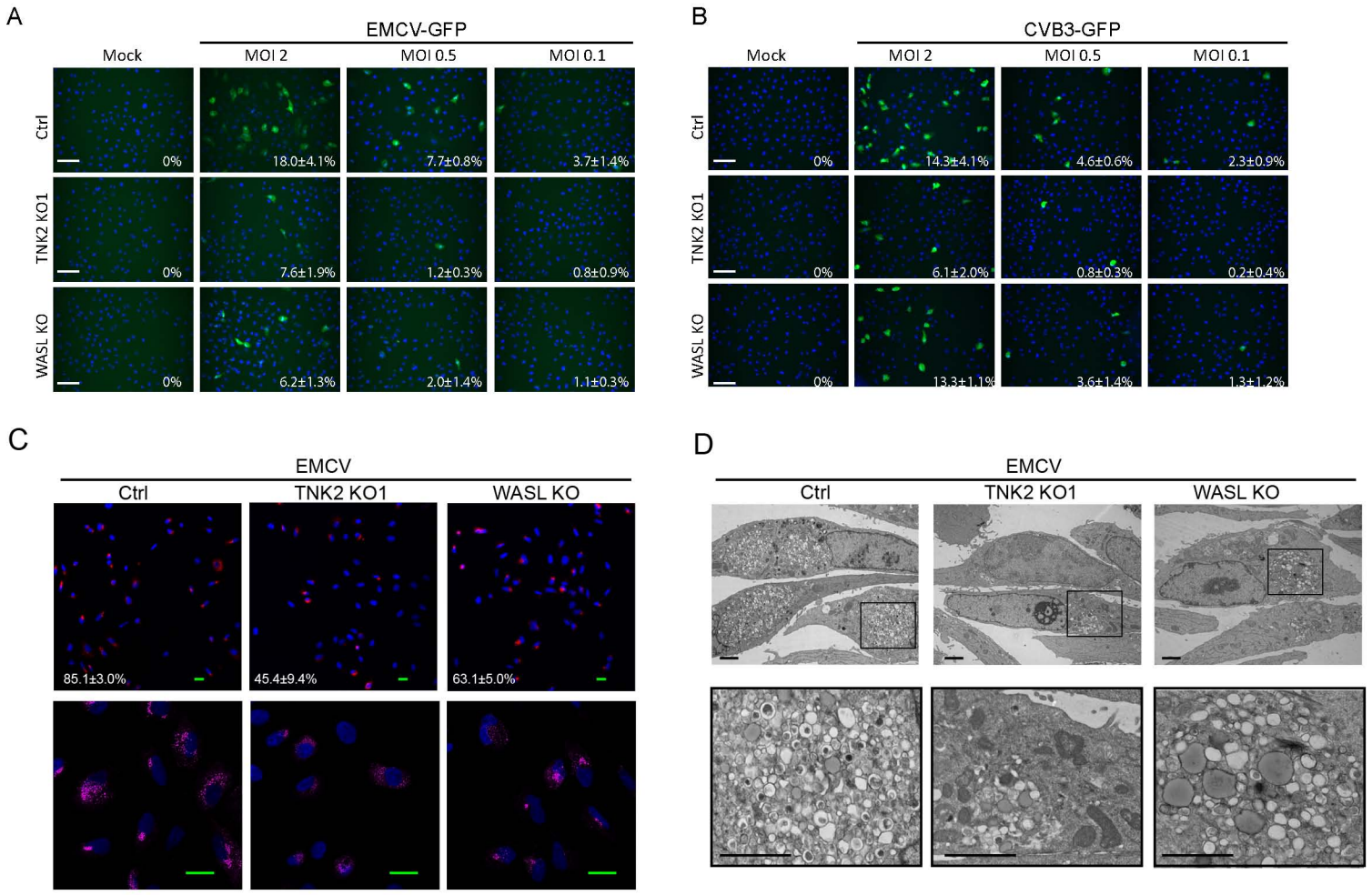

Figure 1-figure supplement1. TNK2 and WASL are critical for multiple picornavirus infection on A549 cells.
(A) EMCV-GFP infection on Ctrl, TNK2 KO1 and WASL KO A549 cells at MOI 2, 0.5 and 0.1. Percentage of positive cells were quantified (values denote mean±s.d., n=3). Scale bars represent 20 μm.
(B) CVB3-GFP infection on Ctrl, TNK2 KO1 and WASL KO A549 cells at MOI 2, 0.5 and 0.1. Percentage of positive cells were quantified (values denote mean±s.d., n=3). Scale bars represent 20 μm.
(C) dsRNA immunostaining of EMCV infection on Ctrl, TNK2 KO1 and WASL KO A549 cells. Percentage of positive cells were quantified (values denote mean±s.d., n=3). Scale bars represent 10 μm.
(D) Electron microscopy detection of EMCV replication complex on Ctrl, TNK2 KO1, and WASL KO A549 cells. Scale bars represent 2 μm.

Figure 1-figure supplement 2

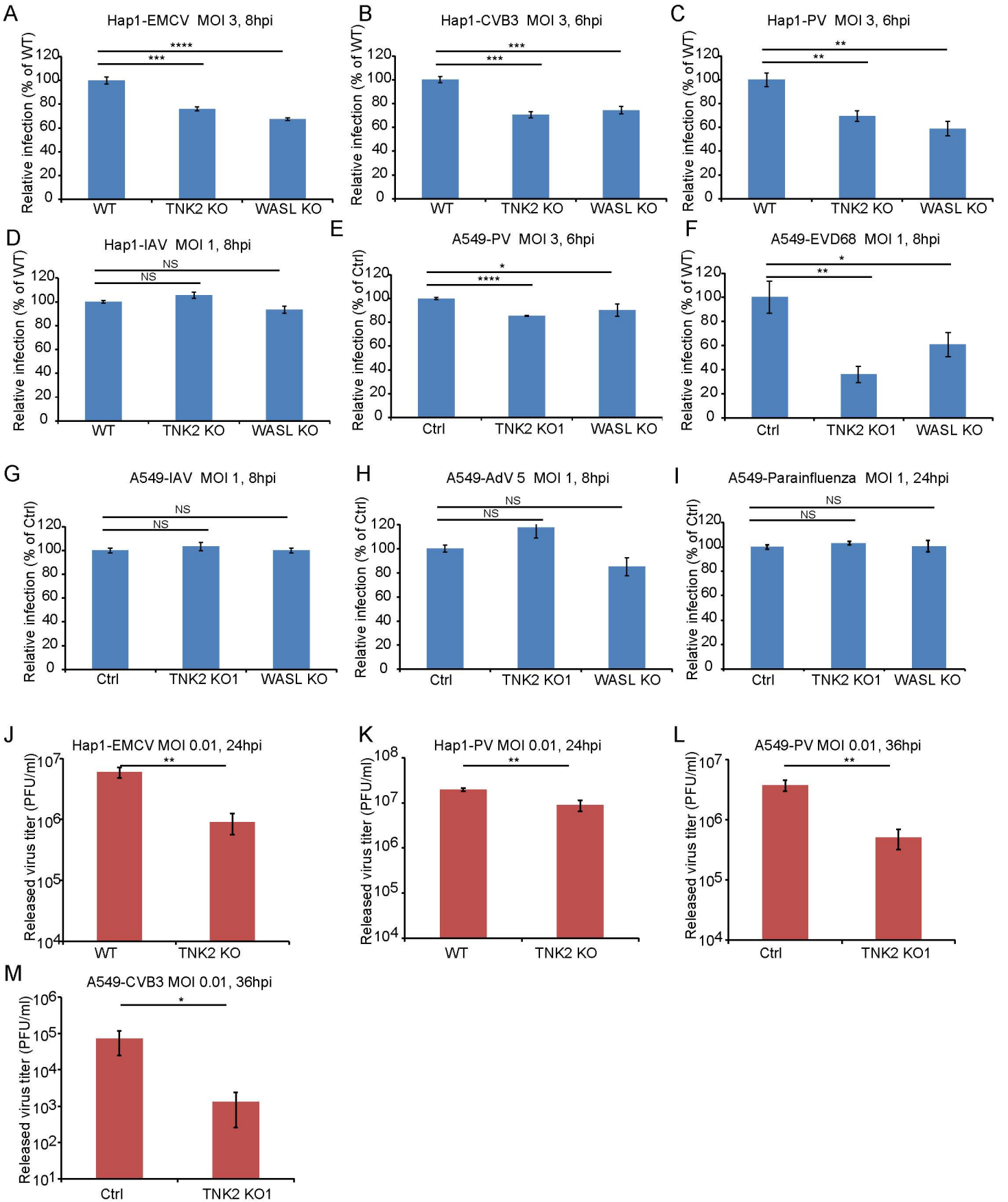

Figure 1-figure supplement2. TNK2 and WASL are critical for multiple picornavirus infection on both A549 and Hap1 cell.
(A-D) FACS quantification of EMCV, CVB3, Poliovirus (PV), and influenza A virus (IAV) virus infection on WT (wild type), TNK2 KO and WASL KO Hap1 cells.
(E-I) FACS quantification of poliovirus (PV), enterovirus D68 (EVD68), influenza A virus (IAV) virus, Adenovirus type 5 (AdV5) and parainfluenza virus infection on Ctrl, TNK2 KO and WASL KO A549 cells.
(J) EMCV growth titration on WT and TNK2 KO Hap1 cells at 24 hours post infection.
(K) Poliovirus growth titration on WT and TNK2 KO Hap1 cells at 24 hours post infection.
(L) Poliovirus growth titration on Ctrl and TNK2 KO1 A549 cells at 36 hours post infection.
(M) CVB3 growth titration on Ctrl and TNK2 KO1 A549 cells at 36 hours post infection.
(A-L) Error bars represent standard deviation of three replicates. The data shown is representative of at least two independent experiments.
*: P<0.05, **: P<0.01, ***: P<0.001, ****: P<0.0001, NS: not significant (P>0.05).

Figure 1-figure supplement 3

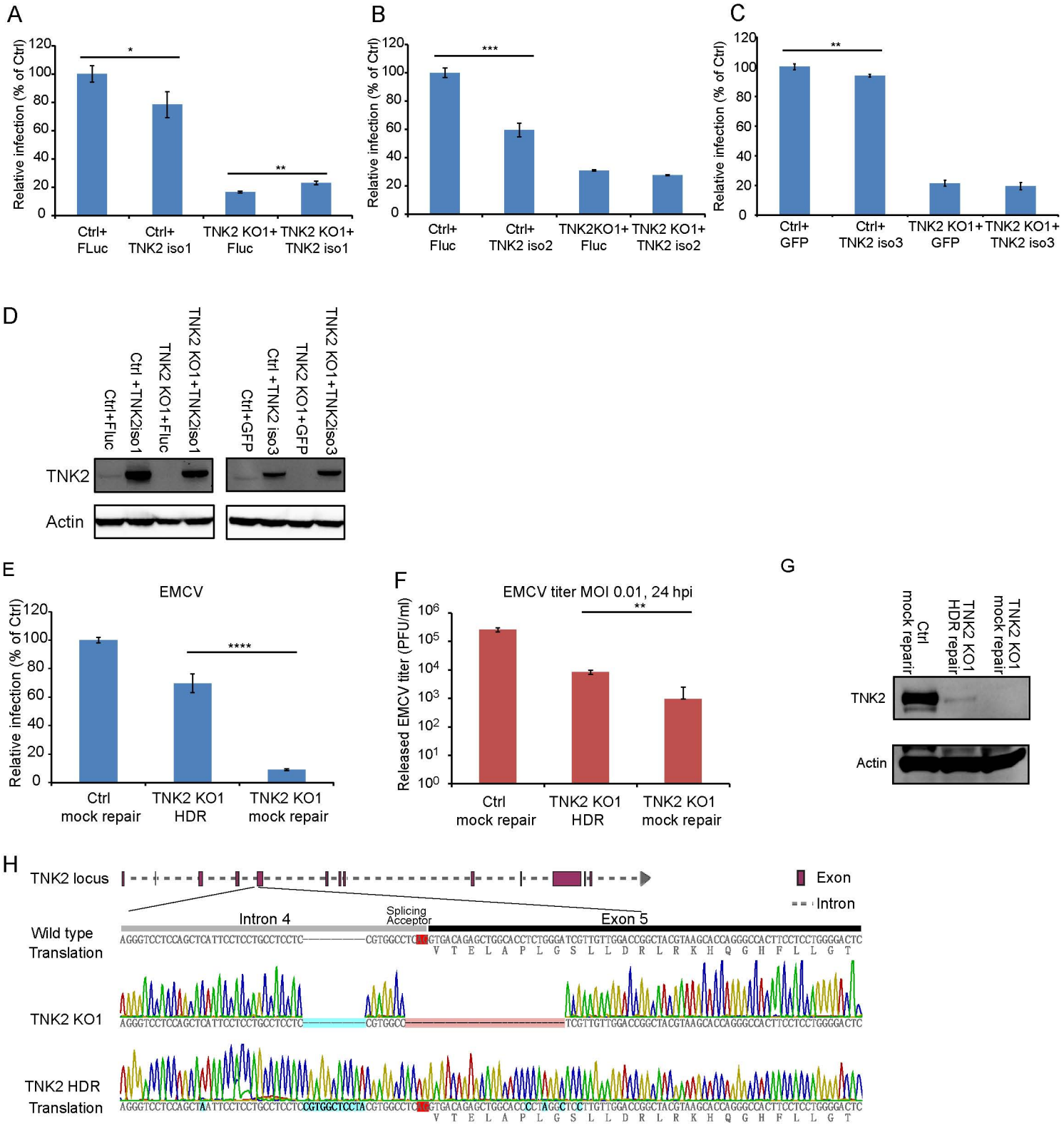

Figure 1-figure supplement3. EMCV virus infection of TNK2 rescue on knockout and control cells.
(A-C) Quantification of EMCV infection on TNK2 KO1 and Ctrl cells transduced with TNK2 isoform 1, 2 and 3 and Fluc. Cells were infected with EMCV at an MOI of 1 and quantified at 10 hours post infection.
(D) Expression of TNK2 in Ctrl and TNK2 KO1 cells transduced with lentivirus expressing TNK2 isoform 1, isoform 3, and Fluc or GFP by Western blot.
(E) FACS quantification of EMCV positive cells for Ctrl mock repair, TNK2 KO1 HDR, and TNK2 KO1 mock repair cells 10 hours post infection at an MOI of 1. Mock repair: cells subjected to the same HDR genome editing but with non-specific targeting sgRNA.
(F) EMCV growth titration on Ctrl mock repair, TNK2 KO1 HDR (homologous template directed recombination), and TNK2 KO1 mock repair cells at 24 hours post infection.
(G) TNK2 protein expression in Ctrl mock repair, TNK2 KO1 HDR cells and TNK2 KO1 mock repair cells. Cells lysates were analyzed by Western blot.
(H) Sequence alignment of TNK2 KO1 cells and TNK2 KO1 HDR (homologous template directed recombination) repaired cells. Splice acceptor is marked with red; synonymous mutations introduced by design and random insertion mutations are marked with blue.
(A-C, E, F) Error bars represent standard deviation of three replicates. The data shown are representative of at least two independent experiments. Fluc: firefly luciferase. *: P<0.05, **: P<0.01, ***: P<0.001, NS: not significant (P>0.05).

Figure 2

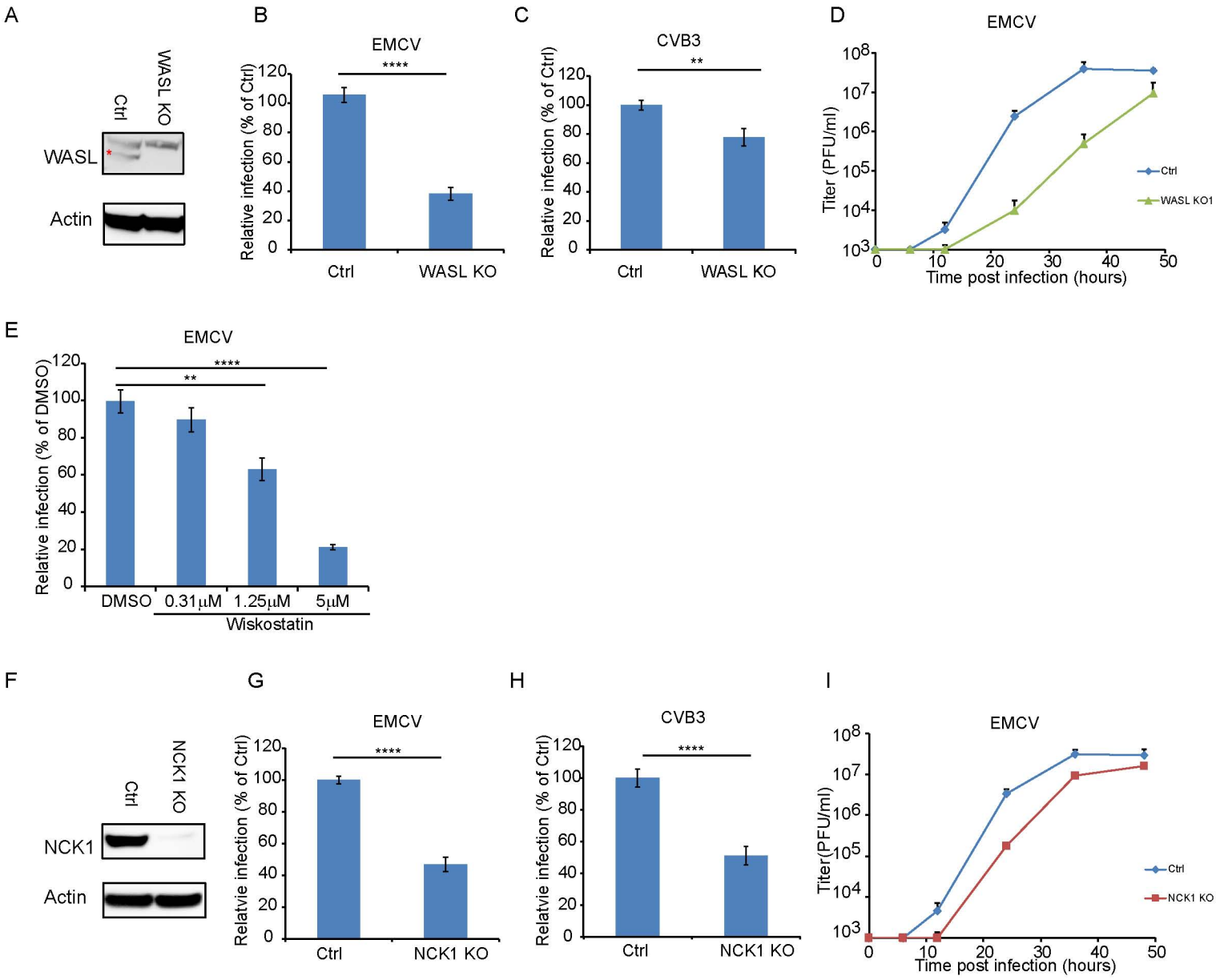

Figure 2. WASL and NCK1 are critical for multiple picornavirus infections.
(A) WASL protein expression in WASL KO and Ctrl cells generated by CRISPR-Cas9 genome editing with either specific targeting or non-specific targeting sgRNA in A549 cells. Cells lysates were analyzed by Western blot.
(B) FACS quantification of EMCV positive cells for WASL KO and Ctrl cells 10 hours post infection at an MOI of 1.
(C) FACS quantification of CVB3 positive cells for WASL KO and Ctrl cells 8 hours post infection at an MOI of 1.
(D) Multi-step growth curve for EMCV multiplication on WASL KO and Ctrl cells infected at an MOI of 0.01.
(E) Wiskostatin inhibition of EMCV infection on naïve A549 cells. A549 cells were pre-treated with Wiskotstatin at indicated concentrations and infected with EMCV at an MOI of 1. Virus positive cells were quantified by FACS.
(F) NCK1 protein expression in NCK1 KO and Ctrl cells generated by CRISPR-Cas9 genome editing with either specific targeting or non-specific targeting sgRNA in A549 cells. Cells lysates were analyzed by Western blot.
(G) FACS quantification of EMCV positive cells for NCK1 KO and Ctrl cells 10 hours post infection at an MOI of 1.
(H) FACS quantification of CVB3 positive cells for NCK1 KO and Ctrl cells 8 hours post infection at an MOI of 1.
(I) Multi-step growth curve for EMCV multiplication on NCK1 KO and Ctrl cells infected at an MOI of 0.01.
(A) The red asterisk indicates WASL protein band. (B, C, E, G, H) Error bars represent standard deviation of three replicates. The data shown is representatives of at least two independent experiments. **: P<0.01, ***: P<0.001, ****: P<0.0001, *****: P<0.00001, NS: not significant (P>0.05).

Figure 2-figure supplement

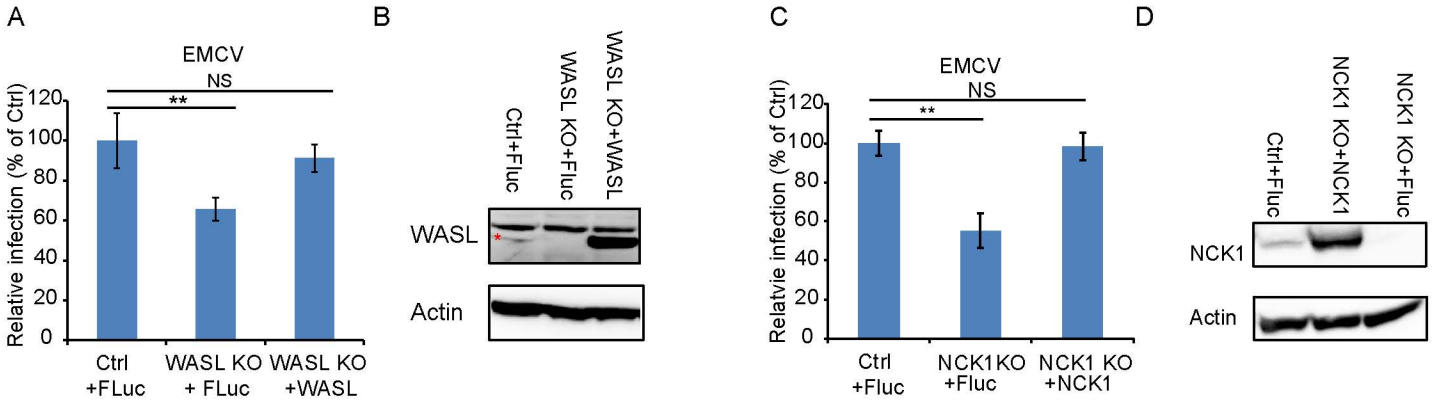

Figure 2-figure supplement EMCV infection of WASL and NCK1 rescued knock out cells
(A) FACS quantification of EMCV positive cells for lentivirus-mediated WASL rescue in WASL KO and Ctrl cells at an MOI of 1. Fluc: firefly luciferase.
(B) Western blot detection of lentivirus-mediated WASL expression in WASL KO and Ctrl cells.
(C) FACS quantification of EMCV positive cells for lentivirus-mediated NCK1 rescue in NCK1 KO and Ctrl cells at an MOI of 1.
(D) Western blot detection of lentivirus mediated NCK1 expression in NCK1 KO and Ctrl cells.
Error bars represent standard deviation of three replicates. The data shown is representatives of at least two independent experiments.
**: P<0.01, NS: not significant (P>0.05).

Figure 3

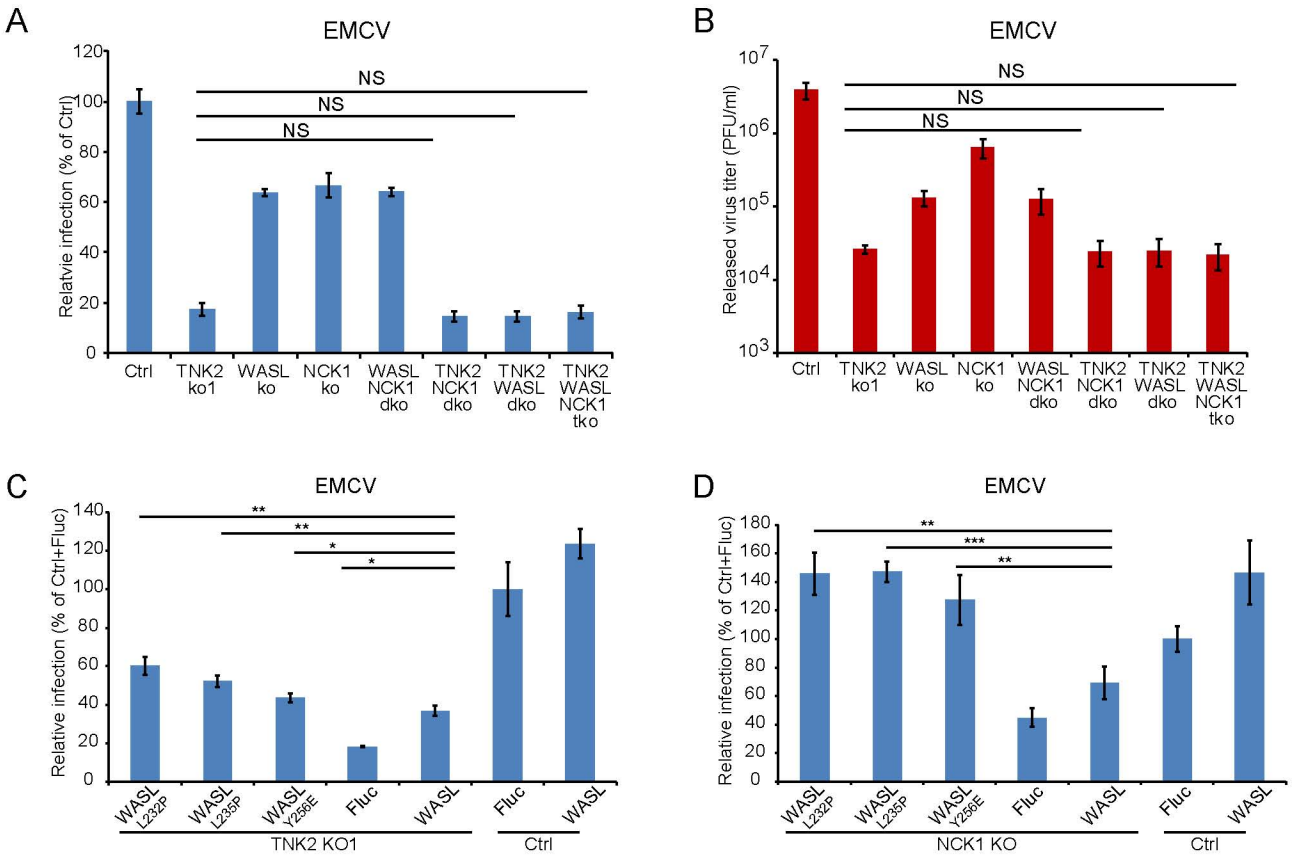

Figure 3. TNK2, WASL, and NCK1 are in a pathway supporting virus infection.
(A) FACS quantification of EMCV positive cells for TNK2, WASL, NCK1 single, double, triple gene knockout and Ctrl cells 10 hours post infection at an MOI of 1.
(B) Virus titer for EMCV multiplication on TNK2, WASL, and NCK1 single, double, triple gene knockout and Ctrl cells at 24 hours post infection at an MOI of 0.01.
(C) FACS quantification of EMCV positive cells for TNK2 KO1 cells that were transduced with constitutively active WASL constructs 10 hours post infection at an MOI of 1.
(D) FACS quantification of EMCV positive cells for NCK1 KO cells that were transduced with constitutively active WASL constructs 10 hours post infection at an MOI of 1.
(A,B) dko: double knockout, tko: triple knockout. (B-D) Error bars for virus infection represent standard deviation of three replicates. The data shown is representatives of two independent experiments.

Figure 3-figure supplement1

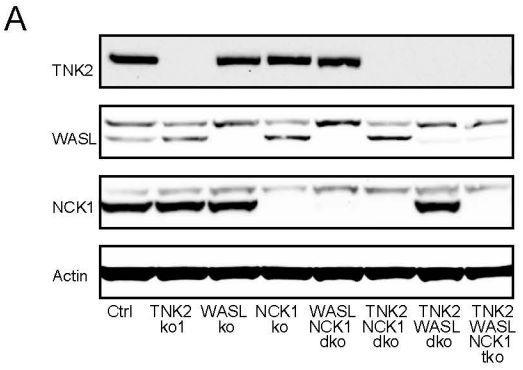

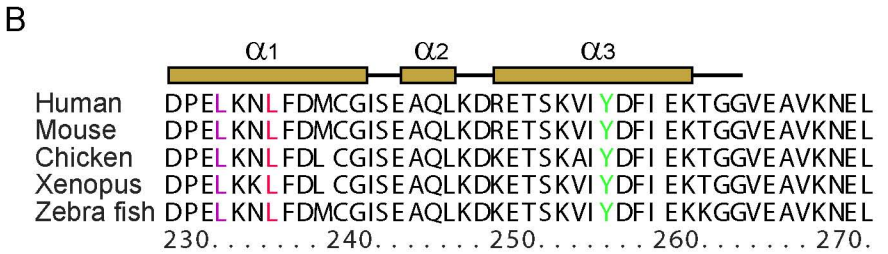

Mutation	Expected function
Wild type	Wild type
L232P	Constitutively active
L235P	Constitutively active
Y256E	Phospho-mimicking

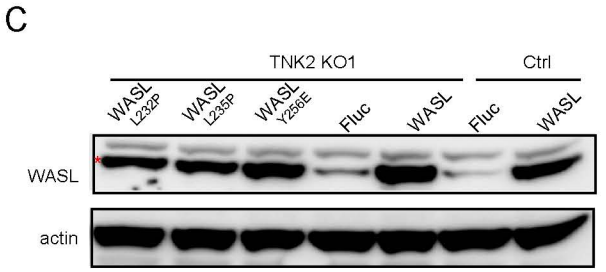

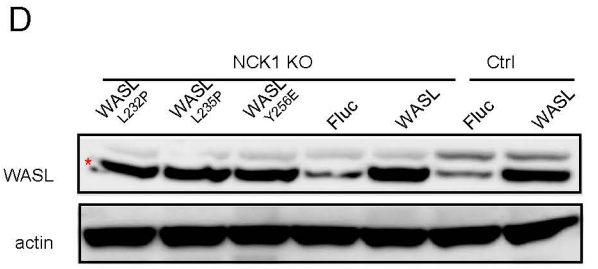

Figure 3-figure supplement1. Gene expression in knock out cells and constitutively active WASL expression.
(A) Western blot detection of TNK2, WASL, and NCK1 expression on single, double, triple gene knockout and Ctrl cells.
(B) Sequence alignment of WASL protein sequences from different vertebrate species. Table indicates specific mutation that have constitutive activity.
(C) Expression of WASL in Ctrl and TNK2 KO1 cells transduced with lentivirus expressing constitutively active WASL, wild type WASL, or Fluc. Cell lysates were analyzed by Western blot.
(D) Expression of WASL in Ctrl and NCK1 KO cells transduced with lentivirus expressing constitutively active WASL, wild type WASL, or Fluc. Cell lysates were analyzed by Western blot.
(C, D) The red asterisks indicate WASL protein band.

Figure 3-figure supplement2

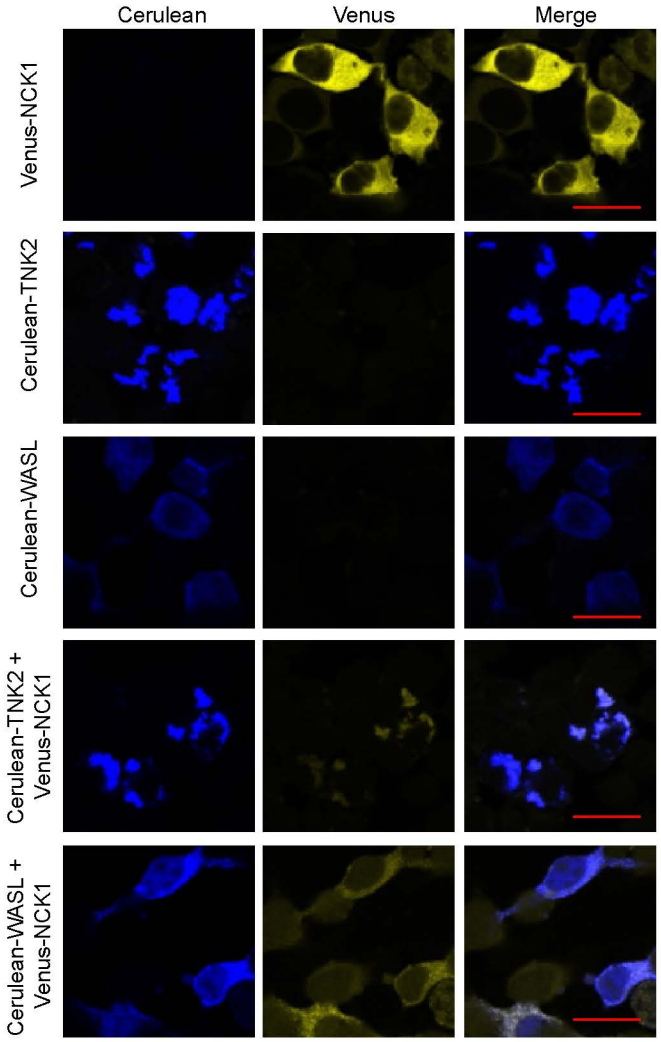

Figure 3-figure supplement2. Co-localization of fluorescently tagged NCK1, TNK2, and WASL expressed in 293T cells by confocal imaging. 293T cells were transfected with Venus-NCK1, Cerulean-TNK2, Cerulean-WASL individually, Venus-NCK1 with Cerulean-TNK2 or Venus-NCK1 with Cerulean-WASL. Cells were imaged by confocal 24 hours after transfection. Scale bars represent 20 μm.

Figure 3-figure supplement 3

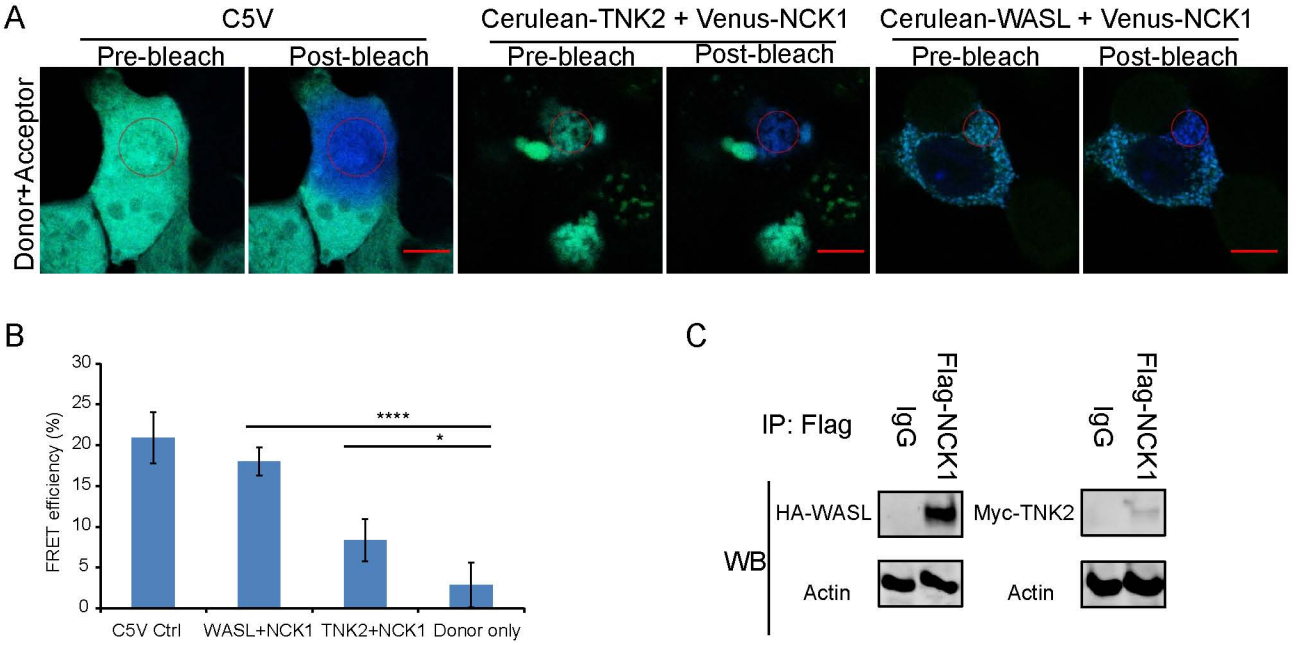

Figure 3-figure supplement 3. TNK2 and WASL directly interact with NCK1.
(A) FRET imaging of C5V positive control, NCK1 and TNK2, and NCK1 and WASL expression in 293T cells before and after acceptor photo bleach. The red circles indicate photo bleached areas. Scale bars represents 10 μm.
(B) Quantification of FRET efficiency of C5V positive control, NCK1 and TNK2, and NCK1 and WASL expression in 293T cells. Error bars for FRET efficiency represent standard deviation of average from four individually bleached images. *: P<0.05, ****: P<0.0001, NS: not significant (P>0.05).
(C) Immunoprecipitation of FLAG-tagged NCK1 with HA-tagged WASL and FLAG-tagged NCK1 with Myc-tagged TNK2.

Figure 4

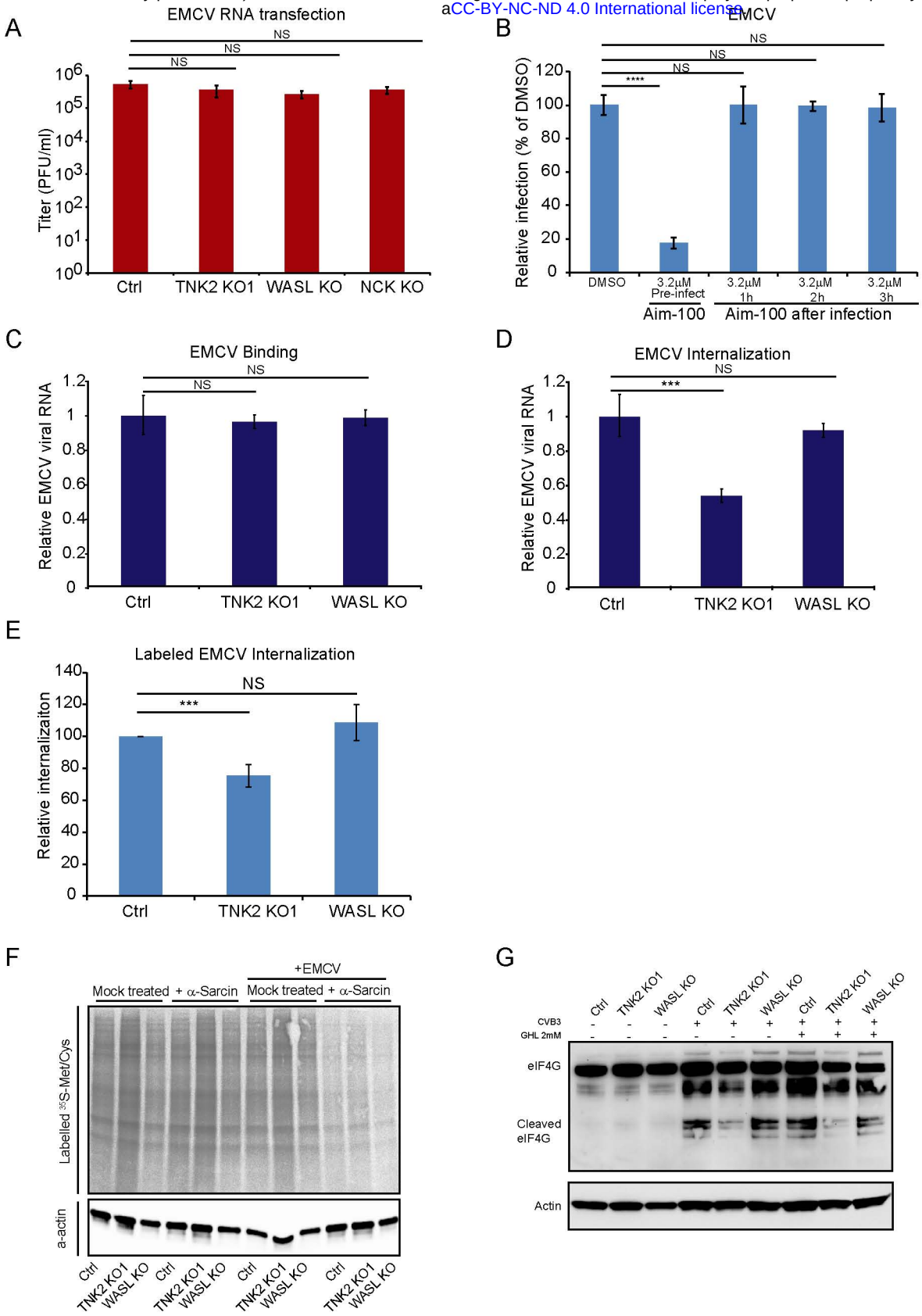

Figure 4. TNK2, WASL, and NCK1 function at an early stage of virus lifecycle.
(A) EMCV released from viral RNA transfected Ctrl, TNK2 KO1, WALS KO, and NCK1 KO cells 10 hours post transfection was quantified by plaque assay.
(B) Time dependent addition of Aim-100 on EMCV infection on naïve A549 cells. A549 cells were treated with 3.2 μM Aim-100 at different time points before and after EMCV infection at an MOI of 1. EMCV positive cells were then quantified by FACS.
(C) Quantification of EMCV virus binding on TNK2 KO1 and WASL KO cells by qRT-PCR expressed as relative change to Ctrl cell binding.
(D) Quantification of EMCV virus internalization in TNK2 KO1 and WASL KO cells by qRT-PCR expressed as relative change to Ctrl cell internalization.
(E) FACS quantification of labeled EMCV internalization in TNK2 KO1, WASL KO and Ctrl cells.
(F) α-sarcin pore forming assay performed on TNK2 KO1, WASL KO and Ctrl cells. Translation was measured by phosphorimaging of 35S-methionine/cysteine incorporation.
(G) eIF4G cleavage by CVB3 infection for 2 hours with or without 2mM guanidine hydrochloride.
(A-E) Error bars represent standard deviation of three replicates. The data shown is representative of two independent experiments. ***: P<0.001, ****: P<0.0001, NS: not significant (P>0.05).

Figure 4-figure supplement

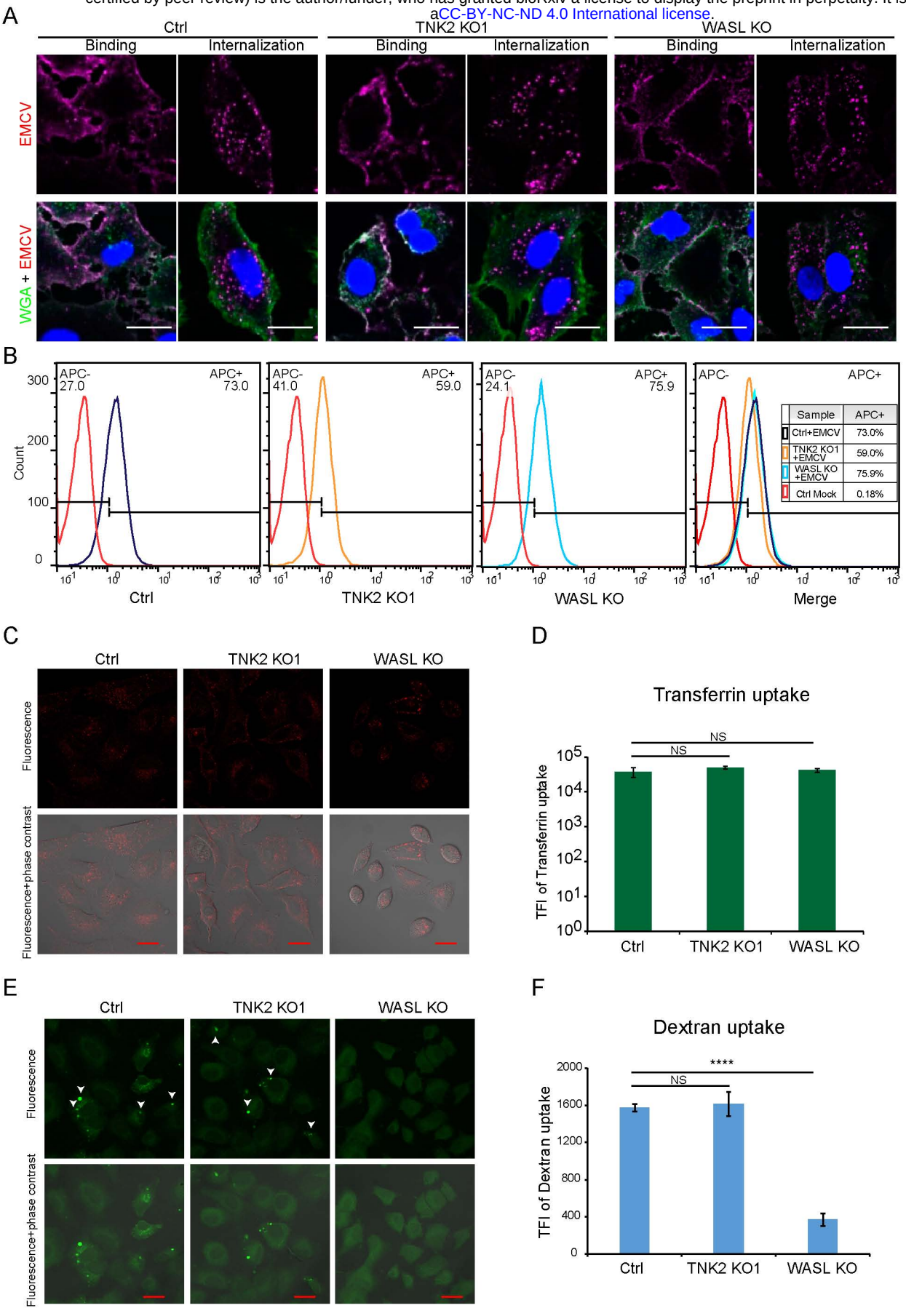

Figure 4-figure supplement. EMCV internalization, transferrin, and dextran uptake in Ctrl, TNK2 KO1 and WASL KO cells.
(A) Labeled EMCV viruses bind and internalize in TNK2 KO1, WASL KO and Ctrl cells. Scale bars represents 20 μm.
(B) FACS plot of labeled EMCV internalization in TNK2 KO1, WASL KO, and Ctrl cells.
(C) Fluorescent images of transferrin uptake in Ctrl, TNK2 KO1, and WASL KO cells. Scale bars represent 20 μm.
(D) Quantification of transferrin uptake by flow cytometry. Error bars represent standard deviation of three replicates. The data shown is representative of two independent experiments. TFI: total fluorescence intensity. NS: not significant (P>0.05).
(E) Fluorescent images of dextran uptake in Ctrl, TNK2 KO1, and WASL KO cells. White arrows indicate macropinosomes. Scale bars represent 20 μm.
(F) Quantification of Dextran uptake by flow cytometry. Error bars represent standard deviation of three replicates. The data shown is representative of two independent experiments. TFI: total fluorescence intensity. NS: not significant (P>0.05), ****: P<0.0001.

Figure 5

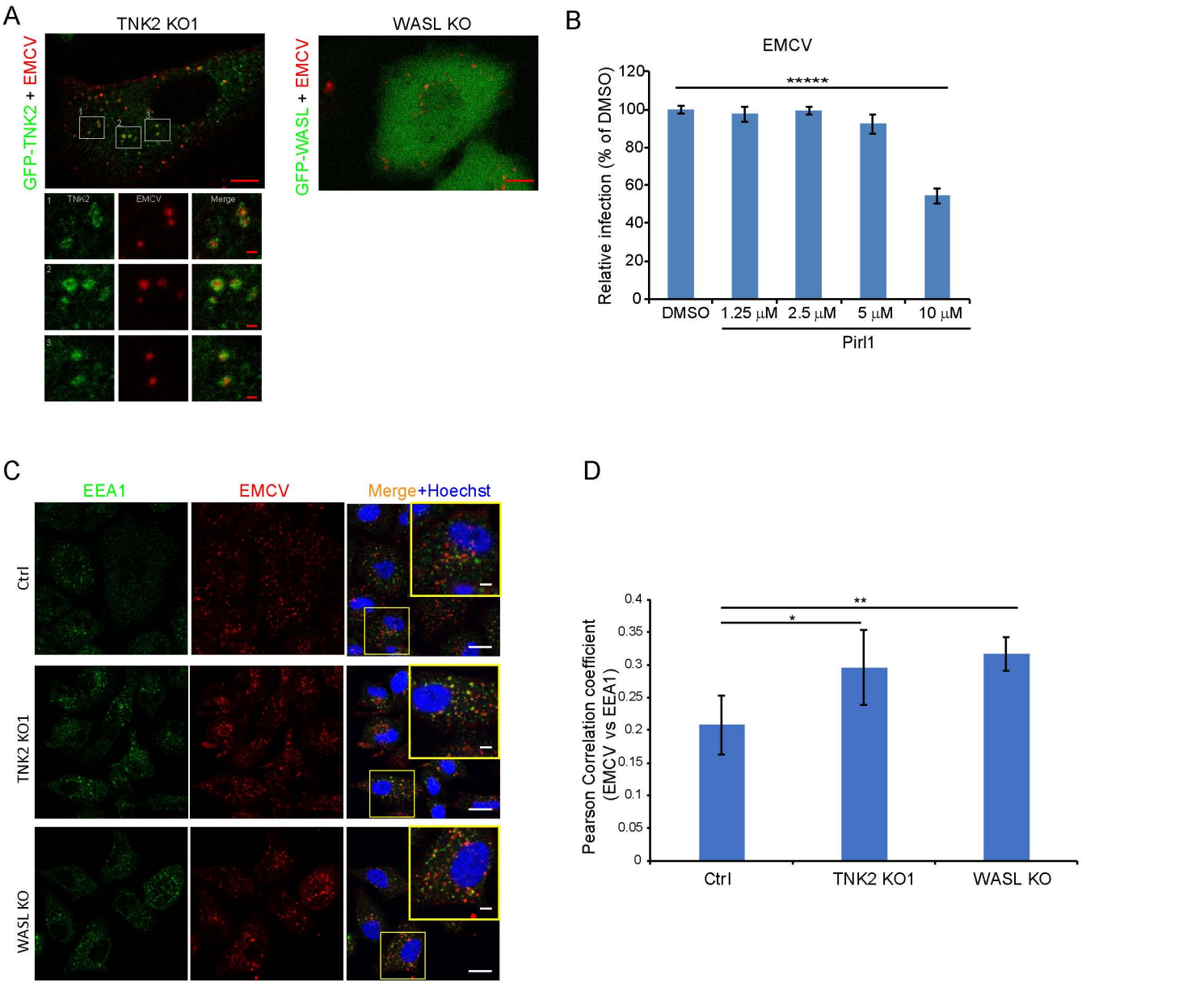

Figure 5. TNK2 mediates virus infection through endosomal trafficking pathways.
(A) Confocal imaging of GFP-tagged TNK2 localization with fluorescently labeled EMCV virus in TNK2 KO1 cells and GFP-tagged WASL localization with fluorescently labeled EMCV virus in WASL KO cells. Scale bars represent 10 μm. Individual channels of different insets were shown. Scale bars represent 2 μm.
(B) FACS quantification of EMCV infection on pirl1 treated A549 cells at 10 hours post infection at an MOI of 1.
(C) EEA1 staining of fluorescently labeled EMCV infected Ctrl, TNK2 KO1, and WASL KO cells. Scale bars represent 20 μm. Insets represent magnification of the boxed region. Scale bars represent 5 μm.
(D) Quantification of Pearson correlation coefficient of EMCV and EEA1 colocalization in Ctrl, TNK2 KO1, and WASL KO cells infected with fluorescently labeled EMCV.
(B, D) Error bars represent standard deviation of three replicates. The data shown is representative of two independent experiments. *: P<0.05, **: P<0.01.

Figure 5-figure supplement

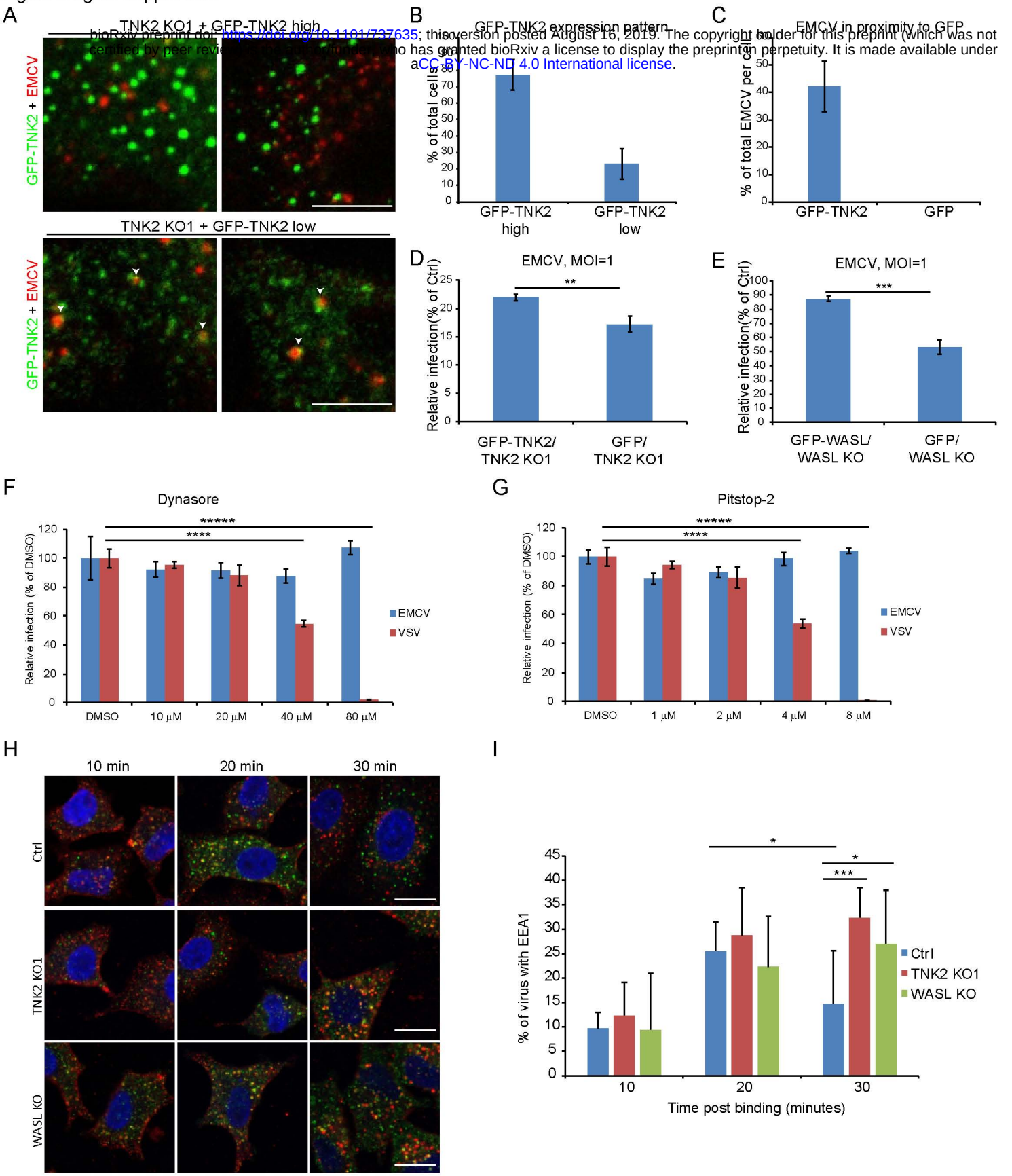

Figure 5-figure supplement. Localization of GFP-TNK2 with fluorescently labeled EMCV.

(A) Fluorescent images of different GFP-TNK2 expression patterns in TNK2 KO1 cells and its localization with fluorescently labeled EMCV. White arrow heads indicate EMCVparticles in proximity to GFP-TNK2. Scale bars represent 10 μm.

(B) Quantification of GFP-TNK2 high and low expression patterns in TNK2 KO1 cells.

(C) Quantification of EMCV particles in proximity to GFP-TNK2 in TNK2 KO1 cells express low GFP-TNK2 compared to EMCV particles in proximity to GFP in TNK2 KO1 cells express GFP.

(D) Quantification of EMCV infection on TNK2 KO1 cells transduced with lentivirus expressing GFP-TNK2 or GFP at 10 hours post infection. Error bars represent standard deviation of three replicates. The data shown is representative of two independent experiments. **:P<0.01.

(E) Quantification of EMCV infection on WASL KO cells transduced with lentivirus expressing GFP-WASL or GFP at 10 hours post infection. Error bars represent standard deviation of three replicates. The data shown is representative of two independent experiments. ***: P<0.001.

(F) Dynasore inhibition of EMCV and VSV infection on naïve A549 cells.

(G) Pitstop-2 inhibition of EMCV and VSV infection on naïve A549 cells.

(H) Fluorescent images of EEA1 co-localization with fluorescently labeled EMCV at 10, 20, and 30 minutes post internalization. Scale bars represent 20 μm.

(I) Quantification of EEA1 co-localization with fluorescently labeled EMCV at 10, 20, and 30 minutes post internalization. Percentage of EMCV co-localized with EEA1 were quantified by image analysis. Error bars represent standard deviation of three experiments. *:P<0.05, ***: P<0.001.

Figure 6

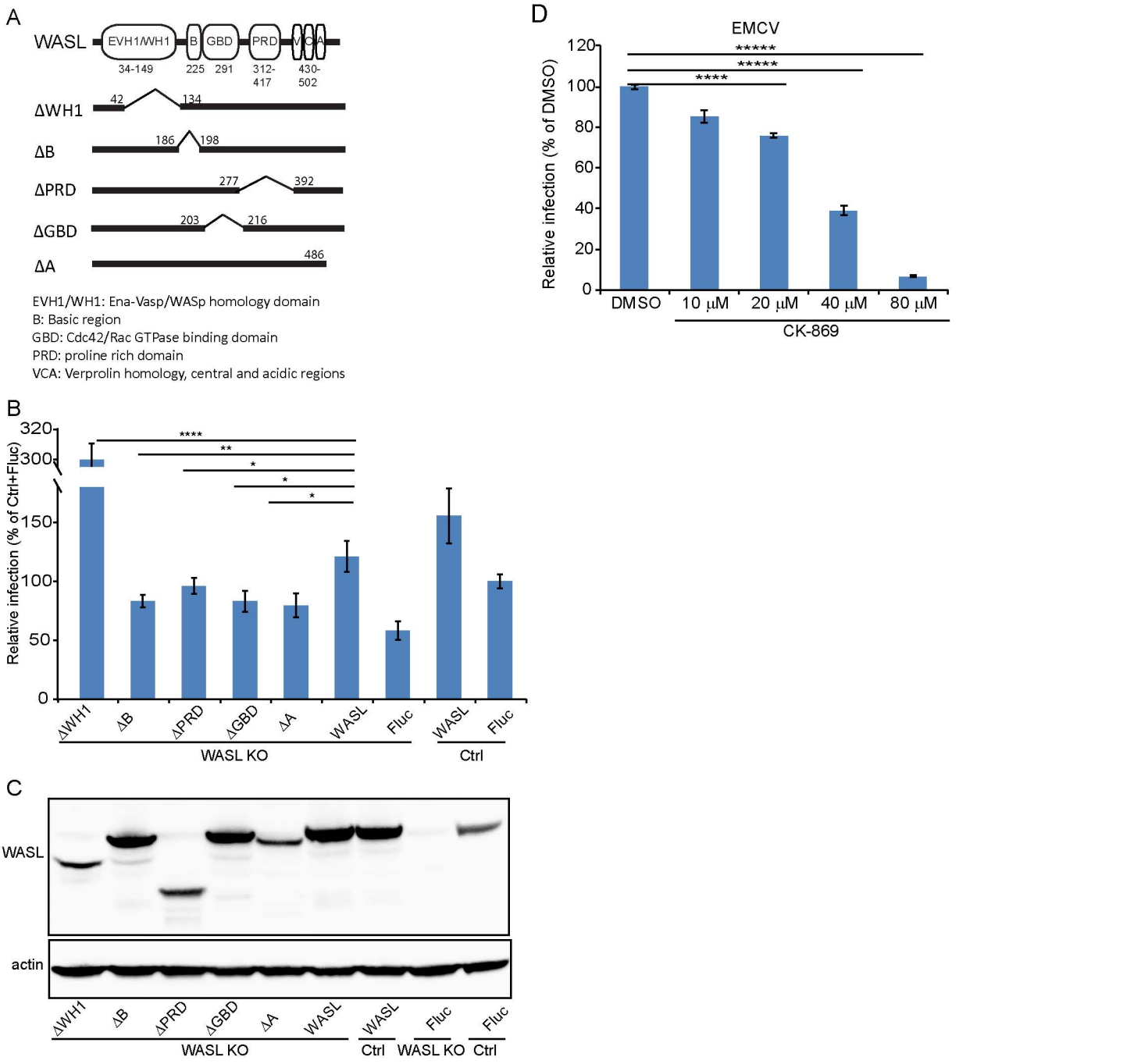

Figure 6. WASL activation and its actin modulation are critical for EMCV virus infection.
(A) Schematic representation of different WASL domain truncations. Each truncation is indicated by amino acid position on the constructs.
(B) FACS quantification of EMCV infection in WASL KO cells transduced with different WASL domain truncations.
(C) Western blot detection of WASL domain truncation expression constructs in lentivirus transduced WASL KO cells.
(D) CK-869 inhibition of EMCV infection on naïve A549 cells at 10 hours post infection at an MOI of 1.
(B, D) Error bars represent standard deviation of three replicates. The data shown is representative of two independent experiments.
*: P<0.05, **: P<0.01, ***: P<0.001, ****: P<0.0001.

Figure 7

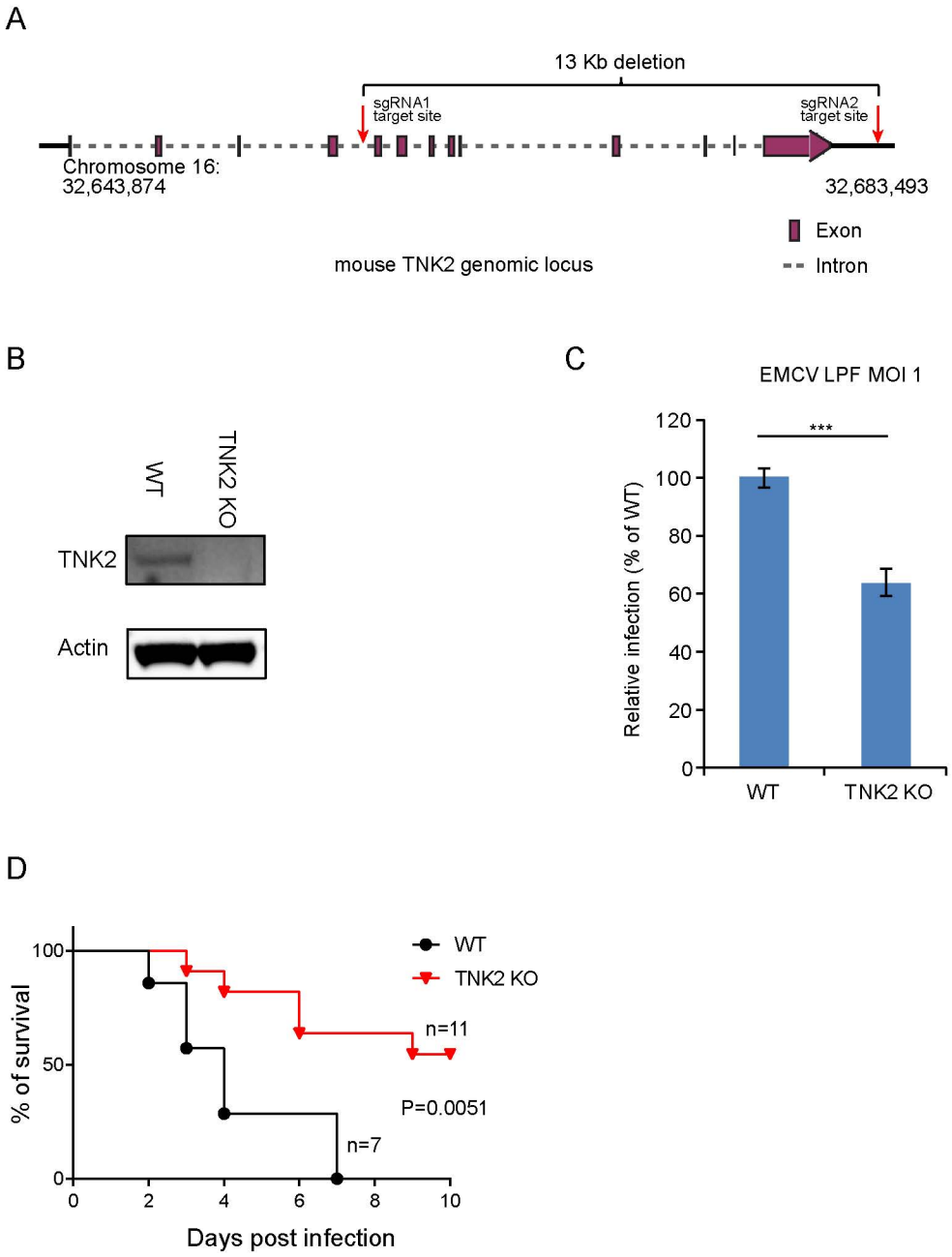

Figure 7. TNK2 is required for EMCV infection in vivo.
(A) Schematic representation of TNK2 knockout design by CRIPSR-Cas9 genome editing in mouse. Exon, intron and genomic position are indicated.
(B) TNK2 expression in mouse primary lung fibroblast cells derived from TNK2 knockout and wild type animals. Cell lysates were analyzed by Western blot.
(C) FACS quantification of EMCV infection in mouse primary lung fibroblast cells derived from TNK2 knockout and wild type animals 6 hours post infection at an MOI of 1. Error bars represent standard deviation of three replicates. The data shown is representative of two independent experiments. ***: P<0.001.
(D) Survival curve of EMCV infection via oral gavage in TNK2 knockout and wild type mice. P=0.0051 by log-rank test.

Figure 8

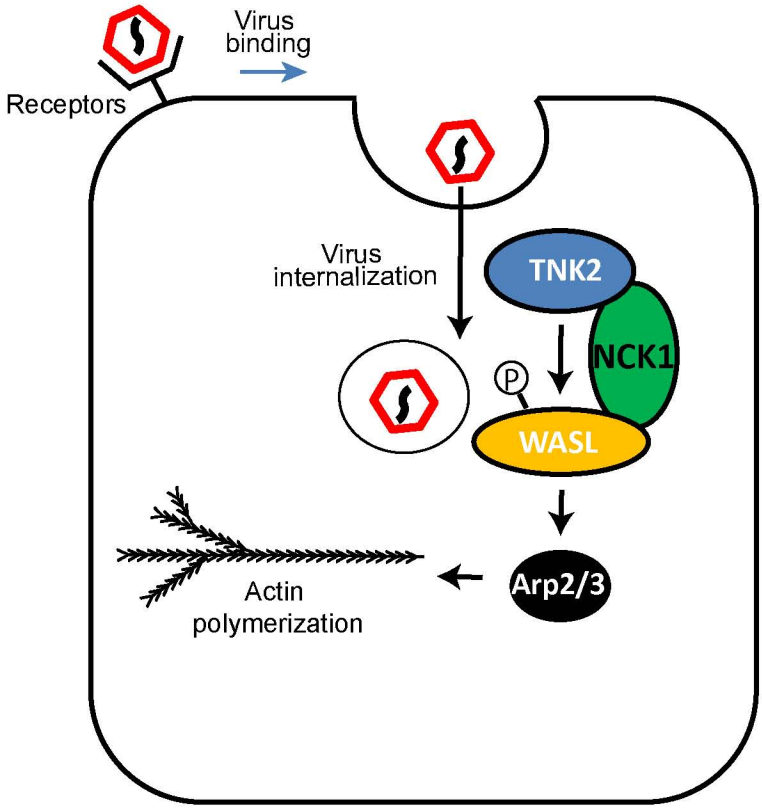

Figure 8. Model of TNK2, WASL and NCK1 function in picornavirus infection.